Unveiling the occurrence of transient, multi-contaminated mafic magmas inside a rhyolitic reservoir feeding an explosive eruption

LITHOS 410–411 (2022) 106574

Contents lists available at ScienceDirect

LITHOS

journal homepage: www.elsevier.com/locate/lithos

Unveiling the occurrence of transient, multi-contaminated mafic magmas inside a rhyolitic reservoir feeding an explosive eruption (Nisyros, Greece)

E. Braschi [a,*], F. Mastroianni [b,c], S. Di Salvo [b], M. Casalini [b], S. Agostini [d], G. Vougioukalakis [e], L. Francalanci [b,*]

[a] Istituto di Geoscienze e Georisorse, sede secondaria di Firenze, Consiglio Nazionale delle Ricerche, Via Giorgio La Pira, 4, 50121 Firenze, Italy
[b] Dipartimento di Scienze della Terra, Università degli studi di Firenze, Via Giorgio La Pira, 4, 50121 Firenze, Italy
[c] Dipartimento di Scienze della Terra, Università di Pisa, Via Santa Maria, 53, I-56126 Pisa, Italy
[d] Istituto di Geoscienze e Georisorse, sede di Pisa, Consiglio Nazionale delle Ricerche, Via G. Moruzzi, 1, 50124 Pisa, Italy
[e] Hellenic Survey of Geology and Mineral Exploration, 3rd Entrance Olympic village 13637, Aharne, Athens, Greece

ARTICLE INFO

Keywords:
Pyroclastic deposits
Compositional heterogeneities
Sr-Nd isotopes
Undercooling textures
Crustal assimilation
Nisyros

ABSTRACT

The investigation of heterogeneous magma systems enhances the understanding of magma differentiation and transfer processes in active volcanoes, thus constraining the dynamics driving the eruptions and the related hazard. Magma heterogeneity is generally preserved in the coeval juvenile products of explosive eruptions, as it occurs in the *Upper Pumice* sequence, emplaced by the last sub-Plinian explosive eruption at Nisyros volcano (Greece). The deposit comprises a basal fallout, overlaid by pyroclastic density current units, followed by a lag-breccia level. White-yellow, porphyritic, rhyolitic pumices constitute the main juvenile component. Grey, crystal-rich juvenile clasts (CRCs) are less abundant (up to 10–15%), and are characterised by three different texture types (Type-A, -B and -C), with specific recurrence in the different depositional units and well correlated to the magma evolution. In the basal unit CRCs occur as andesitic to dacitic lapilli with Type-A and -B vesicular textures associated with highly variable trace element and isotopic compositions. In the lag-breccia deposit, the juvenile clasts occur as bombs with crenulated or bread-crust surfaces, displaying diktytaxitic Type-C textures and less evolved andesitic compositions, covering a larger Nd-isotope range at lower Sr-isotopes compared to the others.

The CRCs are interpreted as the result of the rapid cooling of more mafic magma blobs sequentially intruded in the cooler rhyolitic host magma, in which they attained variable textures by different undercooling conditions, due to their variable compositions. We suggest that a two-stage AFC (Assimilation plus Fractional Crystallisation) process occurred at different pressures, before intrusion in the host magma, accounting for their heterogeneous chemical and isotopic characteristics. Firstly, the most primitive melts variably assimilated gneissic wallrock at depth, acquiring a variable Nd-isotope signature. On the way to the surface, they later experienced shallow AFC processes within different small magma reservoirs, involving heterogeneous carbonate-rocks such as pure limestone, metasomatised marble and skarn. Sequential dynamics of ascent and intrusion into the rhyolitic magma chamber lead the more evolved and skarn-contaminated Type-A and -B melts to firstly move in the upper part of the reservoir to be erupted in the early fallout deposits. Type-C more mafic melts later intruded the rhyolitic reservoir and were erupted in the lag-breccia deposit. The lowest Nd-isotopes recorded by CRCs, with respect to all the volcanic products of the Kos-Nisyros volcanic field, reveal the peculiar transient history for these magmas at relatively shallow levels in the crust. The CO_2 release from the carbonate-rock assimilation has also possibly contributed to trigger the explosive eruption, discharging a large amount of CO_2 into the atmosphere.

1. Introduction

Differentiation processes, storage and transfer of magmas from the source to the surface are among the most studied and debated aspects of active volcanic behaviour, with the aim to constrain the processes driving the eruption style as well as the related hazard.

* Corresponding authors.
E-mail addresses: eleonora.braschi@igg.cnr.it (E. Braschi), lorella.francalanci@unifi.it (L. Francalanci).

https://doi.org/10.1016/j.lithos.2021.106574
Received 20 August 2021; Received in revised form 13 December 2021; Accepted 13 December 2021
Available online 18 December 2021

The study of explosive eruptions allowed researchers to look into volcanic systems, since they represent the primary process through which different portions of a plumbing system and the feeding magma/s are sampled and brought to the surface. Investigating in detail the heterogeneity of the juvenile products generated by these eruptions, and preserved in pyroclastic deposits, is thus crucial to understand the origin of magma variability within the plumbing system, and to infer the magma chamber dynamics prior to the eruption (e.g., Di Salvo et al., 2020; Druitt, 2006; Forni et al., 2016; Francalanci et al., 2014).

In particular, caldera-forming eruptions represent dramatically destructive events generated by the instability of the volcano edifice. Interaction processes between the refilling and resident magmas, the role of crystal mushes, as well as the role of high-pressure processes at deep levels in the crust before their ascent and injection into the magma chamber, are critical in controlling the conditions generating highly explosive activity. In this light, understanding the link between collapse-related explosive eruptions and the possible magmatic trigger, related to a specific magma chamber dynamic, is of paramount importance, and also contributes to determining the possible risk on active volcanoes.

Nisyros (Dodecanese, Greece) is a small active volcano with a relatively young history (since the middle-upper Pleistocene) characterised by two violent explosive, caldera-forming eruptions of Plinian and sub-Plinian type, emplacing thick deposits of pyroclastic material. The last one in particular, named *Upper Pumice* (UP), is recorded in well preserved pyroclastic deposits, showing a high heterogeneity of the juvenile material. This eruption may represent a good case study for understanding heterogeneous magma differentiation and interaction processes involving differently evolved melts, emplaced by a single eruption event. Magma heterogeneity and the occurrence of interaction processes between variably evolved melts are well documented in many other active volcanic systems all over the world (e.g., Unzen, Soulfriere Hills, Kolumbo, Lipari Volcano). The eruption of large volumes of evolved pumices associated with mafic juveniles, or lava flows and domes rich in magmatic enclaves, indicates the occurrence of active refilling of the plumbing system together with peculiar dynamics of the magma chamber (e.g., Davì et al., 2010; Klaver et al., 2016; Plail et al., 2014, 2018; Sato et al., 2017).

We present a detailed study on the variability (textural, geochemical and isotopic) of different juveniles emplaced by the UP eruption of Nisyros volcano, sampled from the relative pyroclastic deposit on several outcrops around the island. Previous papers (Wyers and Barton, 1989; Seymour and Vlassopoulos, 1992; Francalanci et al., 1995; Zellmer and Turner, 2007; Bachman et al., 2012; Klaver et al., 2017, 2018; Popa et al., 2019) considered the UP activity in the frame of the general interpretation of the magmatic evolution of Nisyros volcano. These authors mainly focused on the study of intermediate and evolved products, with only minor attention to the mafic juvenile products that are recurrently erupted during all the recent caldera stage activities, since at least 50 ka. These mafic products are indeed erupted as magmatic enclaves or dense crystalline juvenile clasts, together with the evolved and volumetrically more abundant rhyodacitic/rhyolitic host magmas (i.e., Lodise, 1987; Gansecki, 1991; Braschi et al., 2012; Klaver et al., 2017).

The present work focuses on a detailed study of the mafic crystal-rich clasts (hereafter CRCs) and pumices erupted during the UP activity, combining their evident textural and geochemical variability. We aim to understand the origin of the magma, characterising the plumbing system and the dynamics triggering the last explosive episode of Nisyros volcano. Both aims contribute to improving the knowledge of the petrogenetic processes linked to the occurrence of magma heterogeneities in volcanic systems.

2. Geological and volcanological outline of Nisyros volcano

Nisyros volcano is part of the easternmost volcanic field in the South Aegean Active Volcanic Arc (SAAVA). Its subaerial activity is younger than the 161 ka Kos Plateau Tuff eruption of the nearby Kos volcano (Bachmann et al., 2007; Smith et al., 1996) and has experienced historic phreatic explosions documented in 1871–73 and 1887 CE (Fig. 1). The volcano is built on a basement of Mesozoic limestone and Neogene sediments (Barberi et al., 1988; Varekamp, 1993; Volentik et al., 2002) through two different cycles of activity, forming the present-day composite edifice characterised by a large central caldera depression (about 4 km wide). From the first to the second cycle of activity, the volcanic behaviour of the volcano changes significantly, as well as the compositional characteristics of the erupted magmas. The first cycle (<161–47 ka, Bachmann et al., 2007; Margari et al., 2007) leads to the formation of the volcanic edifice by the emission of lava flows and pyroclastic products with effusive and mild explosive activity. Instead, the second cycle (ca. 47–19.9 ka Margari et al., 2007; Popa et al., 2020) is marked by two Plinian or sub-Plinian, caldera-forming, explosive eruptions (Lower Pumice and Upper Pumice, respectively), emplacing thick deposits of pyroclastic material, both followed by abundant emission of lava flows and domes rich in magmatic enclaves (Nikia and Post-Caldera Domes and lavas) (Davis, 1967; Di Paola, 1974; Wyers and Barton, 1989; Limburg and Varekamp, 1991; Seymour and Vlassopoulos, 1992; Francalanci et al., 1995; Volentik et al., 2002, 2005; Buettner et al., 2005; Vanderkluysen et al., 2005; Longchamp et al., 2011; Braschi et al., 2012; Klaver et al., 2017). In the first cycle, the erupted products show variable degree of differentiation from basaltic-andesites to dacites, with rare rhyolites, alternately emplaced during distinct eruptive events, thus defining recurrent jumps in the degree of evolution along the stratigraphic series (Francalanci et al., 1995). On the contrary, the erupted products of the second activity cycle display evident bimodal compositions with large volumes of highly differentiated magmas (rhyolites and rhyodacites) emplaced together with variable amounts of mafic magmatic enclaves (from basalts and basaltic-andesites to andesites) (Braschi et al., 2012; Francalanci et al., 1995; Klaver et al., 2017, 2018). This points to a dynamic plumbing system in which refilling/refreshing of the magma chamber is the dominant process, generating evident magma immiscibility (Braschi et al., 2012; Francalanci et al., 1995).

The large variability of the rock porphyritic index leads to propose complex magma evolutionary processes for Nisyros magmas, considering its correlation with the Sr isotope ratios (Francalanci et al., 1995). Other authors interpret this variation as discriminant between two magmatic suites (low-porphyritic andesite and high-porphyritic rhyodacite suites), which are considered to evolve along distinct petrogenetic pathways (Klaver et al., 2017, 2018). The evident isotopic variability of Nisyros products is mainly attributed to Assimilation plus Fractional Crystallisation (AFC) processes (e.g., Francalanci et al., 1995; Wyers and Barton, 1989) or to the involvement of a heterogeneous, variably metasomatised, mantle source through time (Braschi et al., 2012; Francalanci and Zellmer, 2019).

The UP eruption is the last explosive magmatic event on Nisyros, recently dated at 46.8 ± 5.7 ka (Margari et al., 2007) and 58.4 ± 2.7 ka (Popa et al., 2020), based on ^{14}C core sample and U-Th on zircon, respectively. Notwithstanding the age uncertainty, stratigraphic relationships indicate that it occurred after the emplacement of the Nikia lava flows and enclaves, and before the final magmatic activity of the post-caldera domes and enclaves (Vougioukalakis, 1993) (Fig. 1). It thus represents an explosive episode, in between two main effusive events, emplacing a relatively large amount of evolved pumices with minor dense and crystal-rich juvenile components (Limburg and Varekamp, 1991).

2.1. The Upper Pumice (UP) pyroclastic succession

The UP succession has been studied in detail since the papers of Limburg and Varekamp (1991), Vougioukalakis (1993) and Hardiman (1999), and recently updated by Volentik et al. (2005) and Longchamp et al. (2011).

The deposits are limited in extent and mainly scattered in the north-

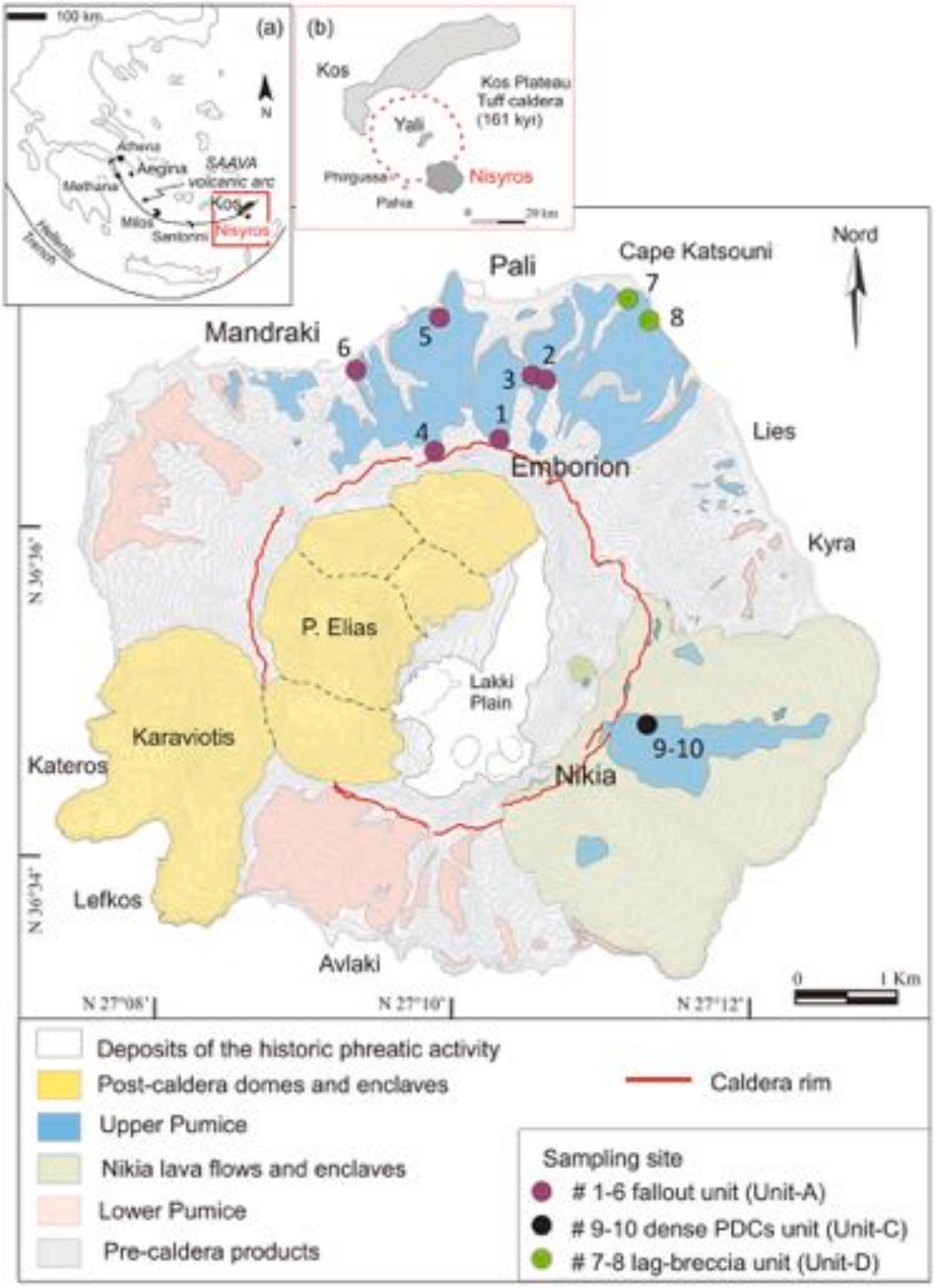

Fig. 1. Schematic geological map of Nisyros volcano (modified from Vougioukalakis, 1993). The distribution of the explosive and effusive products emplaced during the more recent activity of the volcano (<55 ka) is shown, as reported in the legend. The sampling sites are reported in the map and identified by numbers; colours indicate outcrops of different depositional units as shown in legend. More details and the whole sample list are reported in Table1 of Data in Brief, Mastroianni et al., 2021. *Insets*: a) schematic map of the SAAVA area. Nisyros volcano is highlighted in the red box on the eastern side; b) schematic map of the Kos-Nisyros volcanic field with the inferred sub-marine boundary of the Kos plateau tuff caldera dated at 165 ka (modified from Caliro et al., 2005). (For interpretation of the references to colour in this figure legend, the reader is referred to the web version of this article.)

northeast part of the island, with minor outcrops in the south (Fig. 1). The whole succession is only observed in the outcrop near Cape Katsouni. The whole UP succession forms a thick (up to 60 m) pyroclastic sequence that has been subdivided into 6 depositional units (Fig. 2) consisting of: a pumice-rich basal fallout (Unit-A) (Fig. 2a), which is gradually substituted by a pumice-rich, highly diluted pyroclastic density currents (PDC) unit (Unit-B) (Fig. 2b) and by a pumice-rich granular fluid-based dense PDC unit (Unit-C). The latter is overlaid by a pumice-poor breccia-like unit (Unit-D) (Fig. 2c), containing a high amount of lithics (up to 50%) and juvenile crystal-rich bombs, and has been interpreted as a lag-breccia deposit (Limburg and Varekamp, 1991), suggesting the occurrence of eruptive column collapse and subsequent caldera collapse. The sequence is finally capped by two ash-dominated units, interpreted as a dense PDC deposit (Unit-E) and a final phreatomagmatic highly diluted PDC deposit (Unit-F), containing small, probably reworked, pumices in a fine matrix. The basal fallout is the prevalent depositional unit on the northern area of the volcano, where it overlays the Lower Pumice deposit, separated by a paleosoil. The PDCs are typical on the eastern and southern flank of the volcano where they emplaced directly on the Nikia lava flows and older Nisyros products. The lag-breccia unit only outcrops on the east flank near Cape Katsouni.

Longchamp et al. (2011) proposed two possible vent locations for the UP eruption, sited along the actual caldera rim, on the northern side, near Emborion, and on the southern side, near Karaviotis dome,

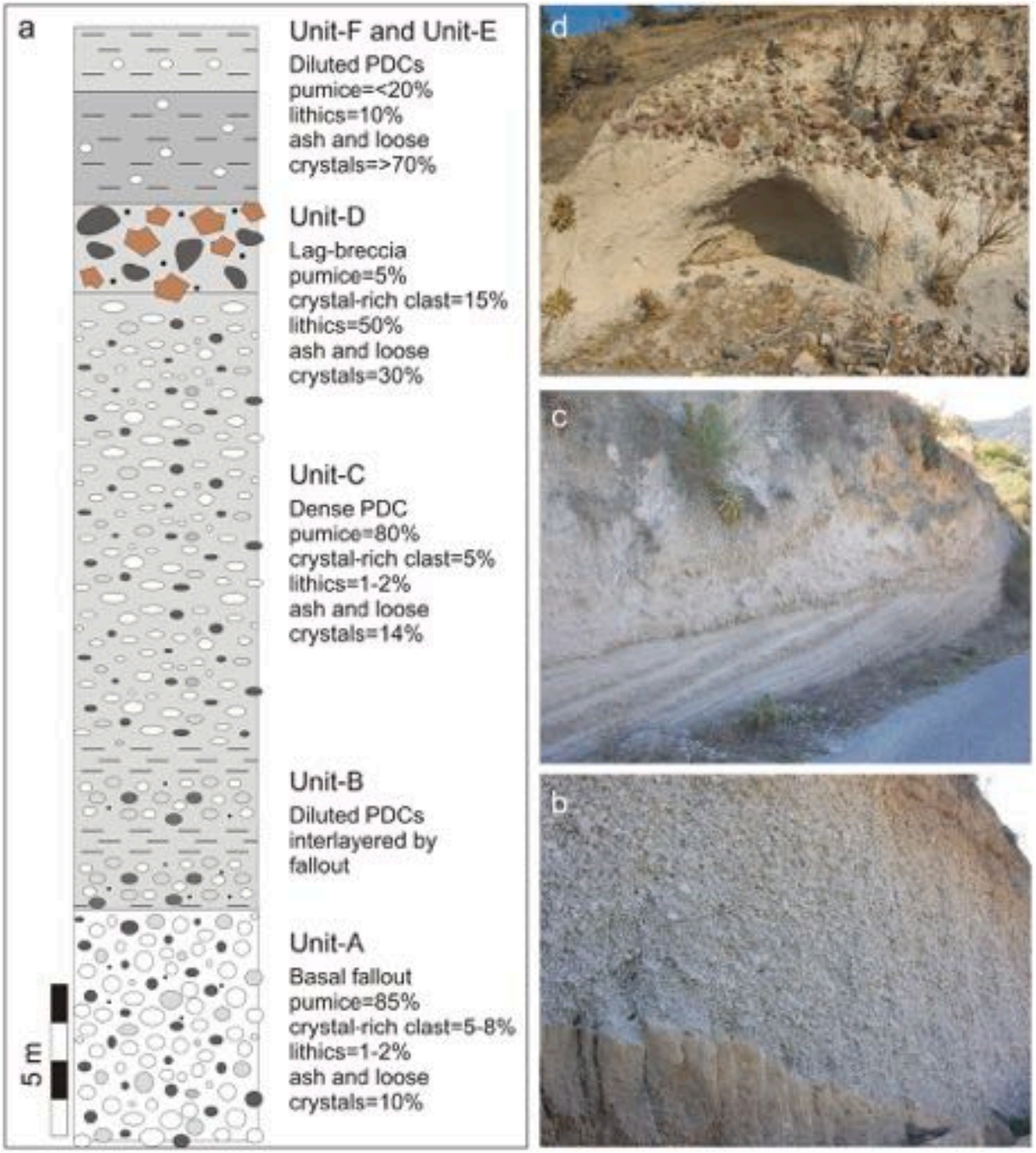

Fig. 2. a) Schematic stratigraphic column of the UP pyroclastic sequence modified from Limbourgh and Varekamp, 1993; b-d) Representative photographs of the principal depositional units: b) basal fallout unit (Unit-A) on the main road near the sampling point 6 of figure1; c) contact between the diluted (Unit-B) and dense (Unit-C) PDC units along the main road to Cape Katsouni; d) lag-breccia unit (Unit-D) at Cape Katsouni close to the sampling point 8.

respectively (Fig. 1). Based on the estimated column height (about 15 km a.s.l.), mass eruption rate (about 2×10^7 kg/s) and volume of the erupted magmas (between 1 and 5×10^8 m^3), the same authors classified the activity as a sub-plinian eruption.

The juvenile components are mainly represented by homogeneous white-yellow pumices forming more than 80 vol% of the basal fallout deposits as well as the overlying PDCs, in association with at least 4–8 vol% of dense Crystal Rich Clasts (hereafter CRCs) that increase up to 15 vol% in the lag-breccia deposit (Fig. 2, 3a,b; Data in Brief, Mastroianni et al., 2021). Minor, generally small (2–3 cm), lithics are dispersed into the basal fallout and intermediate PDC deposits, increasing in size and abundance in the lag-breccia unit.

3. Materials and methods

Detailed observations performed both in the field and on hand-specimens revealed a large variation (in size, colour, density, crystal content and distribution) among the dense CRCs of the UP sequence, as well as much evidence of physical interaction with pumices (Fig. 3c,d), indicating a clear heterogeneity of the erupted magmas during this phase.

To investigate the meaning and origin of the CRCs and their relationship with pumices, we mainly focused on the fallout and lag-breccia depositional units. The fallout unit represents the initial phase of the eruption, with the deposition of the erupted magma directly from the pyroclastic plume. The lag-breccia unit represents the climax of the caldera collapse, with the emplacement of a pyroclastic flow rich in lithic and CRCs.

The fallout unit consists of a 6–8 m thick pumice-rich, well-sorted deposit (Fig. 2a) with sub-angular pumice clasts ranging in size from 10 to 40 cm and minor percentages of CRCs, ranging in size from 2 to 3 cm (e.g., Fig. 3a) to 25–30 cm. A large variability in shape, colour, density and crystal content is observed in the CRC population of each fallout outcrop. They can occur as: i) grey, highly vesiculated, coarse-grained clasts (e.g., Fig. 3a); ii) grey and salt-and-pepper dense, coarse- to fine-grained clasts; iii) light grey, glass-rich, spongy clasts (Data in Brief, Mastroianni et al., 2021).

The lag-breccia unit is limited to a single outcrop on the north-eastern part of the island, south of Cape Katsouni. It is a 3 m thick deposit composed of a fine, yellowish ash matrix containing a high abundance of lithic fragments, ripped from the hydrothermal system, together with many (at least 15 vol%) dark, dense, crystal-rich clasts and bombs (Figs. 2d and 3b). Few pumices are also present.

Sampling was carried out with care collecting all of the different varieties of juveniles observed on each outcrop of the Upper Pumice deposits for a total of 94 samples (Table 1 of Data in Brief, Mastroianni et al., 2021). Pumices were sampled from each single location to explore the possible variability within the evolved component (16 samples) (Fig. 1). The CRCs were collected according to their textural and physical variability observed in the field (density, colour, crystal content), in order to maximize the detail and representativeness of sampling and to explore the recurrence of different juvenile types among the outcrops (78 samples, some of which have been further subdivided in laboratory).

3.1. Analytical methods

Thirty-one selected samples were prepared for whole rock geochemical analyses. Sample selection was conducted on the basis of

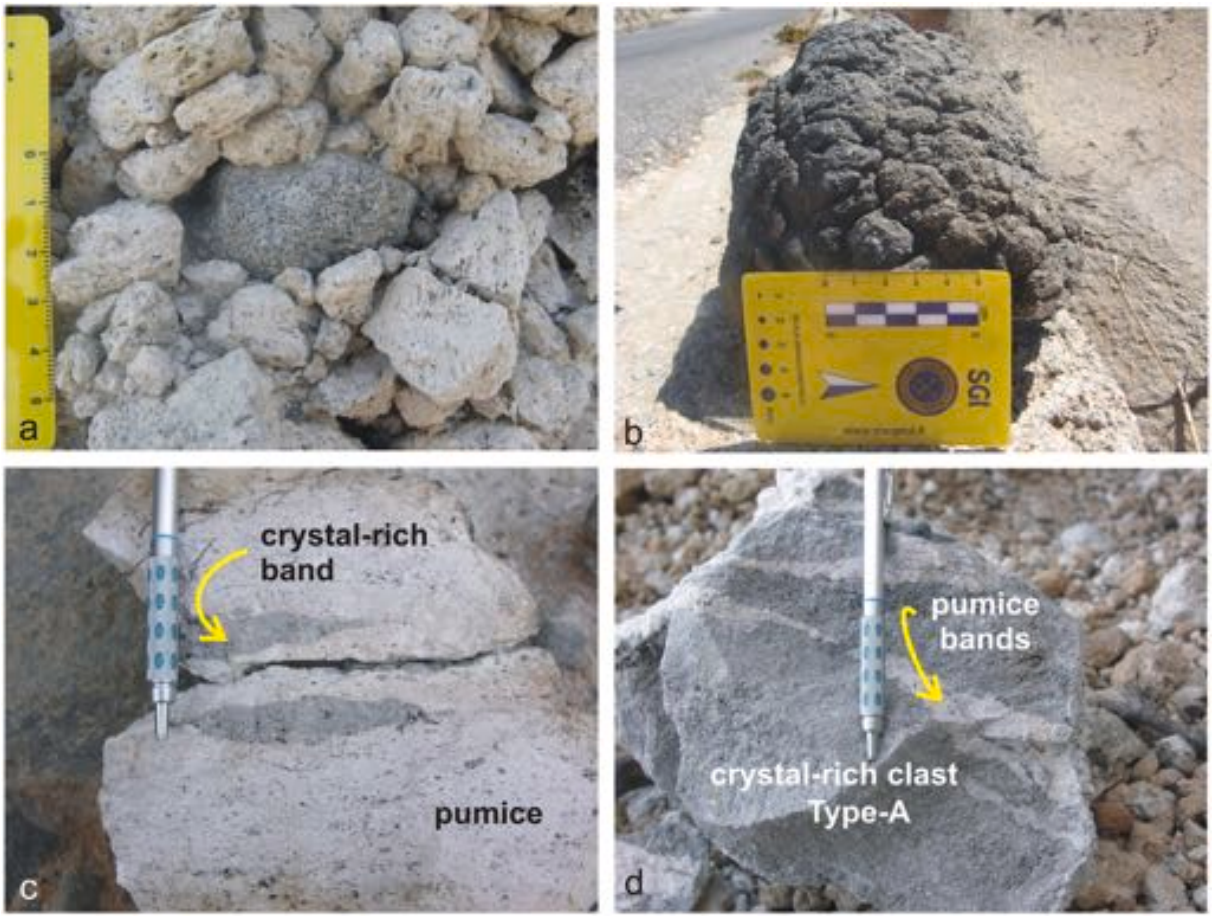

Fig. 3. Representative photographs showing details of: a) centimetric, vesiculated CRC in the basal fallout, surrounded by light pumice lapilli; b) pluridecimetric, dense CRC of the lag-breccia unit with clear crenulated surface; c-d) banded pumice and CRC testifying the mechanical interaction between the two lithologies.

their size and freshness in order to achieve representative data. CRCs <10 cm in diameter and pumices with marked evidence of micro-mingling were excluded. Analytical results are fully reported in tables and figures of the Data in Brief (Mastroianni et al., 2021) and hereafter named Table-DB and Figure-DB.

Major and trace elements were performed at the Actlabs Laboratories (Ancaster, Ontario). Results are reported in Table-DB 2.

Sample preparation for Sr-Nd isotopic analyses were performed on 20 further selected samples at the Radiogenic Isotope Laboratory of the Earth Sciences Department of the University of Florence (DST-UNIFI) following the standard digestion and elemental purification procedures described by Avanzinelli et al. (2005) using suprapure quality acids. Before digestion, each sample was leached using diluted (1 N) HCl acid and rinsed with Milli-Q water.

Sr isotope measurements were carried out using a Thermal Ionization Mass Spectrometer (TIMS, Thermo-Fisher TritonTi) at the DST-UNIFI, following conditions and methods described in Avanzinelli et al. (2005) for whole rocks samples. Nd isotopes were measured at the Radiogenic Isotope Laboratory of the IGG-CNR of Pisa using Multi-collector Inductively Coupled Plasma Mass Spectrometer (MC-ICPMS, Thermo NEPTUNE Plus). Results, analytical accuracy and reproducibility are reported in Tables-DB 2 and 9.

Mineral chemistry and glass composition were obtained at the Electron Microprobe Laboratory of the IGG-CNR of Florence, using a Jeol JXA-8600 superprobe with 15 kV of acceleration voltage, 10 nA of beam current and variable counting times for major and minor elements. Results were reported in Table-DB 3–8 and showed in Supplementary Material (Fig. S1).

4. Results

4.1. Textural and mineralogical characteristics of the UP juvenile components

Pumice samples have homogenous porphyritic texture, with up to 5 vol% of phenocrysts (0.5–1 mm) and microphenocrysts (0.1–0.3 mm) mainly composed of plagioclase with minor orthopyroxene and oxides. Plagioclase phenocrysts are poorly zoned with composition ranging between $An_{30–40}$; orthopyroxenes have monotonous composition with Mg# 0.58–0.59. Rare microphenocrysts of clinopyroxene (Mg# 0.70) and amphibole are also found, usually as fragments (Table-DB 4–8). The glassy groundmass is clear with rare microlites of plagioclase and in places shows a typical fluidal, highly vesiculated fabric (Fig. 4a,b). Glomeroporphyritic aggregates and micro-enclaves are also present (Fig. 5a,b).

On the contrary, the CRCs show a strong heterogeneity in textures, vesicularity and glass content, which reflects the large physical variability observed at hand-specimen (Fig. 4c-h). They consist of 65–85 vol % of crystals (Fig. S1) and contain a low content (< 5–10 vol%) of phenocrysts (up to 1 mm in size), showing evident disequilibrium textures, and multi-phase glomerocrysts. Their groundmasses are all hypocrystalline with highly vesiculated glass and evident variation in crystal size (0.1–0.5 mm) and distribution.

Despite this textural variability, all the CRCs show a similar mineralogical assemblage. Plagioclase (60 to 80 vol% of the mineral assemblage) is present as phenocrysts and as fine, tabular or acicular crystals forming the microcrystalline groundmass network. Orthopyroxene (10–15 vol%) is mostly found as single crystal in the groundmass or in aggregates. Clinopyroxene (up to 5 vol%) is generally present as microphenocryst. Amphibole (up to 30 vol% in many samples but not ubiquitous) can be found associated with plagioclase to form the microcrystalline groundmass network, either with acicular or tabular habitus, or as reaction rims on pyroxenes. Amphibole is ubiquitous in the lag-breccia CRCs where it forms the crystalline network with plagioclase. Variable opaques content (up to 5 vol%) and rare, small resorbed olivines are also present.

Evident variations are observed in the relative abundances and recurrence of the different phases among the studied samples. Plagioclases of the microcrystalline network are usually clear and normally zoned, whereas phenocrysts commonly show resorbed-dusty sieved cores with clear rims. Plagioclases and orthopyroxenes have large compositional ranges with $An_{33–89}$ and Mg# between 0.54 and 0.81, respectively. Orthopyroxenes are more abundant than clinopyroxenes (Mg# 0.66–0.72) and display normal zoning (Table-DB 4–8).

On the basis of petrographic and backscattered (BSE) observations from the Scanning Electron Microscope (Figure-DB 15, 17, 18, 21), the CRCs can be grouped into three different types, namely Type-A, Type-B and Type-C (Fig. 4c-h).

Type-A (Fig. 4c,d) clasts are generally characterised by microcrystalline texture with almost equigranular crystal size (0.1–0.5 mm), constituted by tabular plagioclases, amphiboles and pyroxenes (mainly orthopyroxene), with variable oxides content. Many crystals are clearly broken and dispersed in a glassy, highly vesiculated groundmass, without a defined fabric. The glass of the groundmass is clear and characterised by rounded or occasionally elongated vesicles, which are defined by thin sects of glass, similar to those observed in the pumice (except for the fluidal textures) (Fig. 4a). In some cases, aggregates formed by plagioclase and resorbed orthopyroxene, often recrystallised into clinopyroxene or amphiboles, are present. Single plagioclase phenocrysts, characterised by sieved core are also present. Type-A is the prevalent crystal-rich juvenile found directly in contact with the pumice (Figs. 2c and 5). The contact is usually sharp and characterised by single-crystal disaggregation and micro-scale dispersion of the crystal-rich portion into the pumice, often as micro-enclaves (Fig. 5c,d). Type-A samples are typically found in the fallout deposits, rarely in the lag-breccia level.

Type-B (Fig. 3e,f) clast samples show a microcrystalline, inequigranular, low porphyritic texture, with variable crystal orientation defining in places a sort of network, likely the Type-C textures (see description below). They are characterised by the same mineralogical paragenesis and general crystal-size range as Type-A. The relative amount of crystals, glass and vesicles as well as their distribution are highly variable within Type-B samples, generating a spectrum of textures between those of Type-A and Type-C (Fig-DB 12). They are mostly found in the fallout and PDC deposits, but some of them were also collected from the lag-breccia unit.

Type-C (Fig. 4g,h) includes quite dense, crystal-rich clasts characterised by a peculiar network formed by acicular crystals of plagioclase, amphibole, interstitial pyroxene and variable opaques content. The grain size is variable from 0.1 to 0.5 mm and roughly equigranular. They have diktytaxitic voids in the groundmass and show low glass content and variable vesicle abundance, generally lower than the other types (Table-DB 1). Acicular diktytaxitic textures are interpreted as the result of the rapid cooling of magma as it came in contact with a cooler, more evolved host (Bacon, 1986; Blake, 1990; Blake and Fink, 2000). Some of them show aggregates composed by plagioclase, subhedral, partially resorbed pyroxene and olivine crystals, sometimes with evident recrystallisation into amphiboles. Type-C samples are mainly found in the lag-breccia deposit, and only occasionally in the fallout.

4.2. Geochemistry and Sr-Nd isotopes of the UP juvenile components

All the juvenile products erupted by the UP activity belong to the calc-alkaline series and display a single trend of correlation between silica and K_2O (Fig. 6). A compositional gap between 64 and 69 wt% SiO_2 discriminates the evolved rhyolitic pumices from the CRCs population, which vary from andesite to dacite (Fig. 6 and Table-DB 2).

Pumices show homogeneous composition with very low variations in the silica content (70.5–71.6 wt%), except for a single sample belonging to a proximal deposit of the fallout unit with lower SiO_2 content (69.0 wt %). They only show slight variations in some trace elements (Figs. 7,8), which are not correlated with stratigraphy or with their distribution

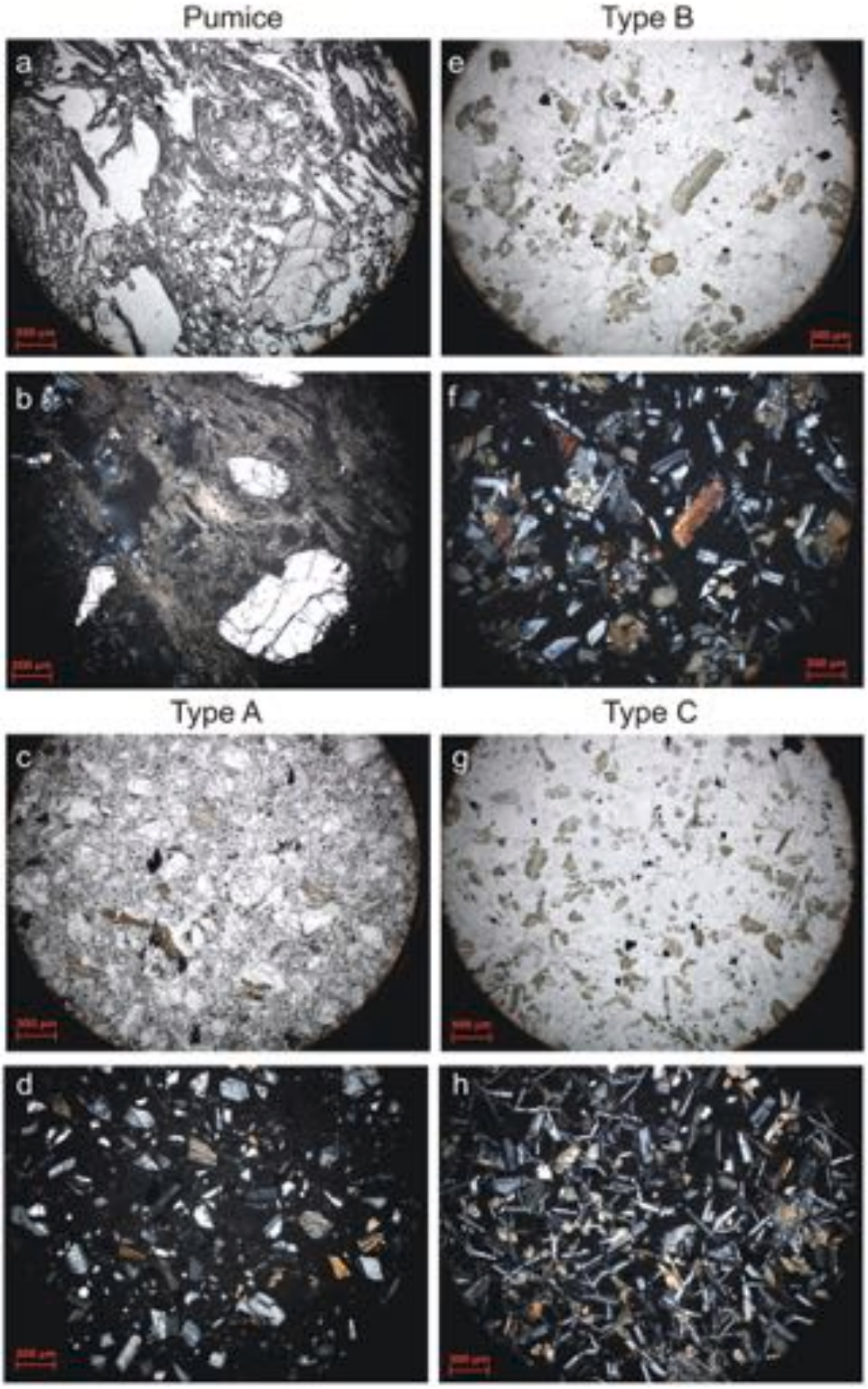

Fig. 4. Representative micro-photographs in plane and cross polarized light of pumice (a-b) and CRC samples (c-h). The three different types of CRCs namely Type-A (c-d), Type-B (e-f) and Type-C (g-h), are compared on the basis of their textures as described in the text.

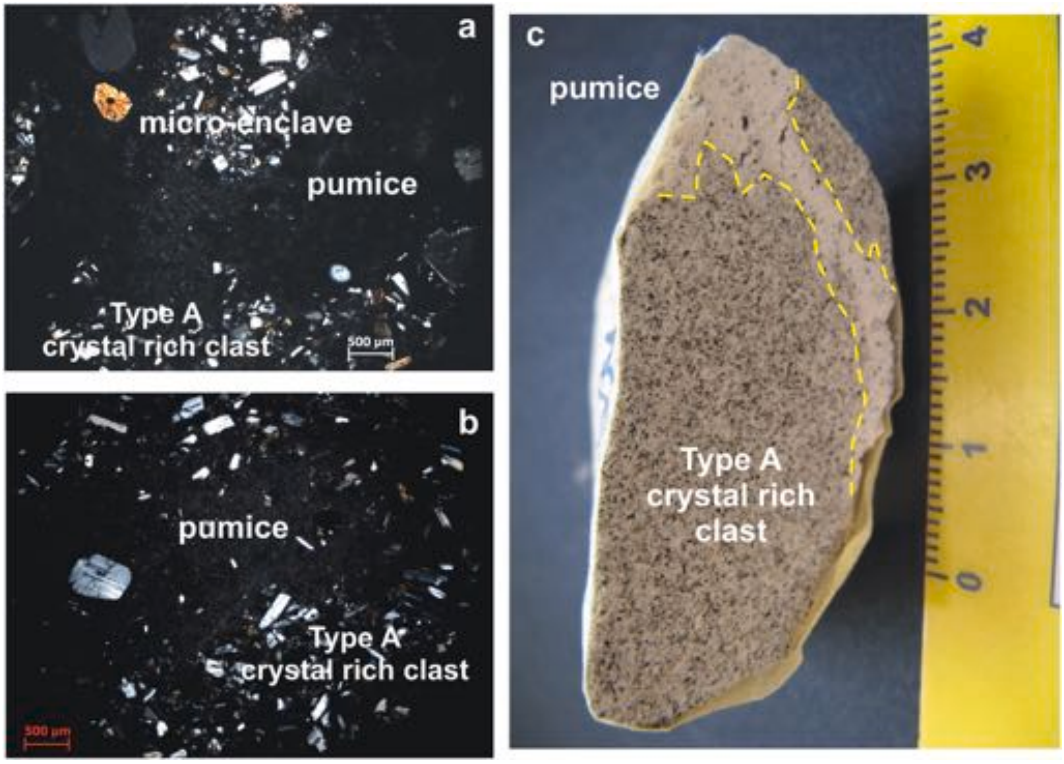

Fig. 5. Representative photomicrographs in cross-polarized light (a, b) showing the sharp contacts, micro-mingling and banding between pumices and CRCs, compared to the corresponding hand-specimen fragment (c).

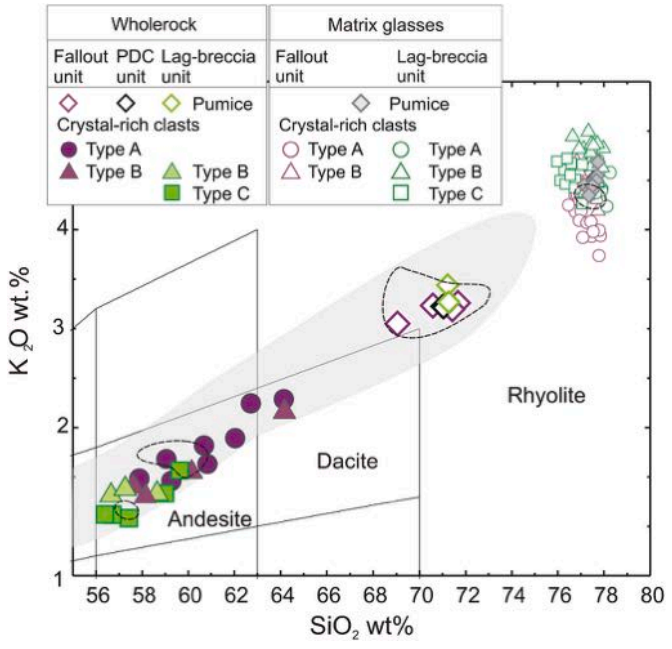

Fig. 6. K_2O–SiO_2 classification diagram (Peccerillo and Taylor, 1976) of whole rocks and glasses of the UP pumices and CRC samples, discriminated on the basis of the relative depositional units (colours) and textures (symbols). Data (wt%) are reported on water free-basis. The grey shaded field represents the whole compositional variability of Nisyros volcanic rocks; light-blue dashed fields represent the composition of the UP juveniles as reported in literature (data from Francalanci et al., 1995; Francalanci et al., 2005 and references therein; Buettner et al., 2005; Zellmer and Turner, 2007; Tomlinson et al., 2012; Klaver et al., 2018). (For interpretation of the references to colour in this figure legend, the reader is referred to the web version of this article.)

among the different outcrops.

CRCs show a wider variability in major and trace element contents than pumices, with silica ranging from 56.4 to 64.2 wt%. Type-A and Type-B samples from the fallout cover almost the whole compositional range, whereas Type-C samples from lag-breccia are less variable and less evolved (from 56.4 to 59.6 wt% of SiO_2) (Figs. 6, 7). Most of major (MgO, FeO, CaO and Al_2O_3) and compatible element contents (i.e., Co, Sc, V) describe a general, negative correlation with silica (Fig. 7), whereas the behaviour of the other major elements and of trace elements is more heterogeneous.

TiO_2, P_2O_5, Na_2O, High Field Strength Element (HFSE) and Rare Earth Element (REE) define two, scattered but consistent, positive correlations with silica (Trend-1 and Trend-2, highlighted by different colours from Fig. 8b-f onwards). Notable, both trends develop from distinct primitive compositions that belong to the CRCs erupted in the lag-breccia unit, and mainly represented by Type-C (Fig. 8a,b). These samples show significant trace element heterogeneity, despite their low silica variability. Along both trends, HFSEs and REEs, together with TiO_2, P_2O_5, Na_2O contents, steeply increase in the more evolved samples, which correspond to the Type-A and Type-B clasts, found in the fallout unit (Figs. 8, 9a,b). The two trends are not well defined by Large Ion Lithophile Elements (LILE), with a possible exception of Sr, which is also negatively correlated with silica (Fig. 9c,d). Eu/Eu* is negatively correlated with the evolutionary degree in both trends, whereas Tb_N/Yb_N shows a decrease from 56 to 62 wt% of silica, followed by a rough increase towards the highest silica contents only in Trend-2 (Fig. 9e,f).

The matrix glass compositions, analysed on some selected pumice and CRC samples, largely overlap with silica content ranging from 76 to 78 wt% (Fig. 6; Table-DB 3). However, as observed for the whole-rock composition, the pumice glasses are more homogeneous than the CRC glasses, which also show slight differences between the CRCs of lag-breccia and those of the fallout deposit (see also Supplementary Material).

Sr and Nd isotopes of pumices are uniform and cluster around

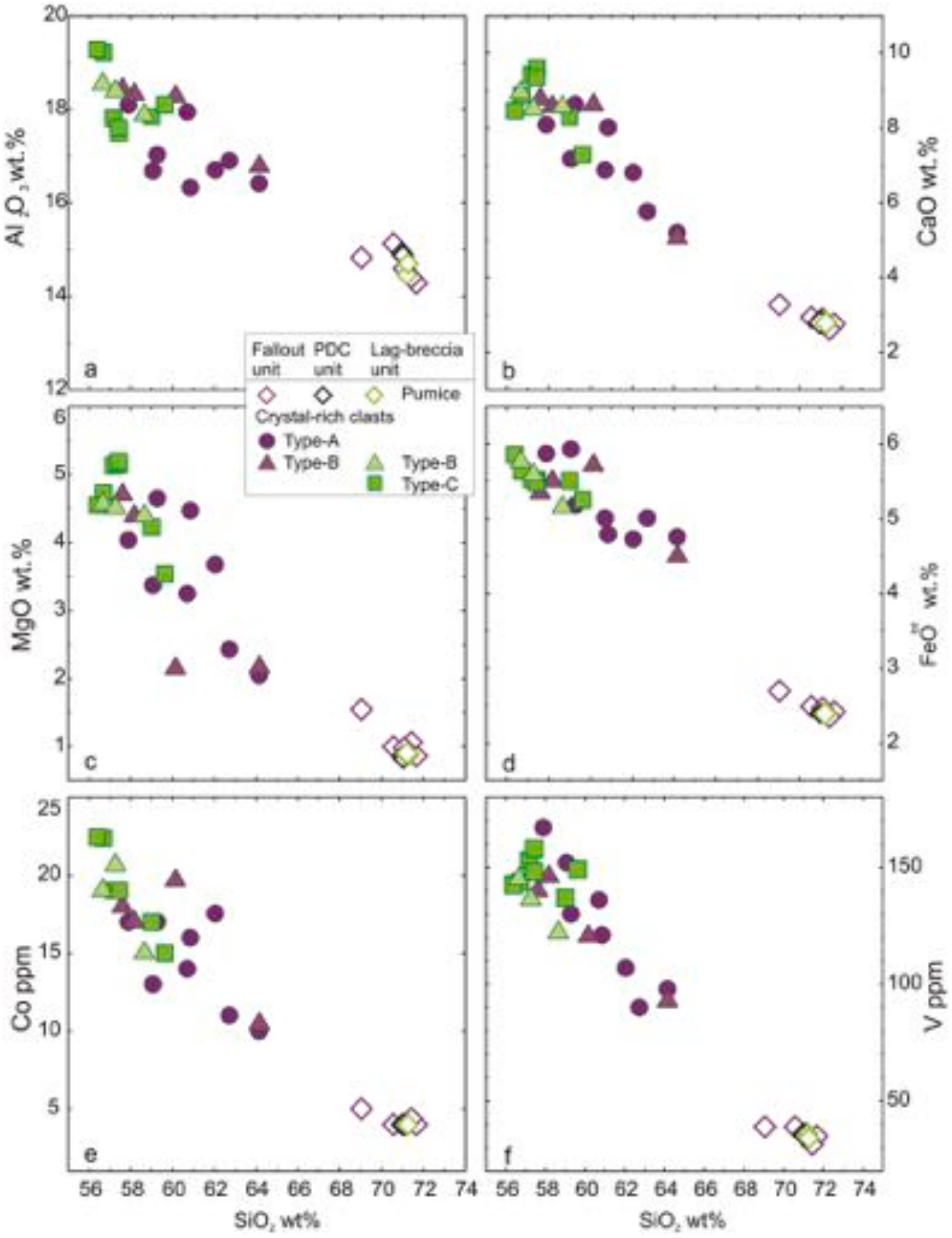

Fig. 7. Variation diagrams of representative major (wt%) and compatible trace (ppm) elements versus silica for the UP pumice and CRC samples. Major elements are reported on water free-basis. Symbols and colours follow the same rationale of Fig. 6.

0.70454 and 0.51262, respectively (Fig. 10). On the contrary, Sr- and Nd-isotopes analysed on CRC samples, are largely variable with $^{87}Sr/^{86}Sr$ between 0.70420 and 0.70488 and $^{143}Nd/^{144}Nd$ between 0.51251 and 0.51262, overlapping the isotope signature of pumices. It is noteworthy that the CRCs show significantly lower $^{143}Nd/^{144}Nd$ values than the other Nisyros products with $SiO_2 < 60$ wt% and most of them even have the lowest $^{143}Nd/^{144}Nd$ values registered for the Nisyros-Kos-Yali volcanic field products (Fig. 10a), only similar to those recorded in the western part of the South Aegean volcanic arc (Francalanci and Zellmer, 2019 and reference therein).

Different isotopic variations are registered in the fallout and in the lag-breccia CRCs. The lag-breccia clasts show small $^{87}Sr/^{86}Sr$ variability encompassing the whole $^{143}Nd/^{144}Nd$ range, defining quite a steep negative correlation. On the contrary, the fallout CRCs display the entire $^{87}Sr/^{86}Sr$ range, coupled with a more restricted $^{143}Nd/^{144}Nd$ variation, depicting an almost flat trend (Fig. 10a).

Within the two trends defined by trace element variations (Fig. 8), Sr-Nd isotopes are largely variable suggesting that multiple evolutionary

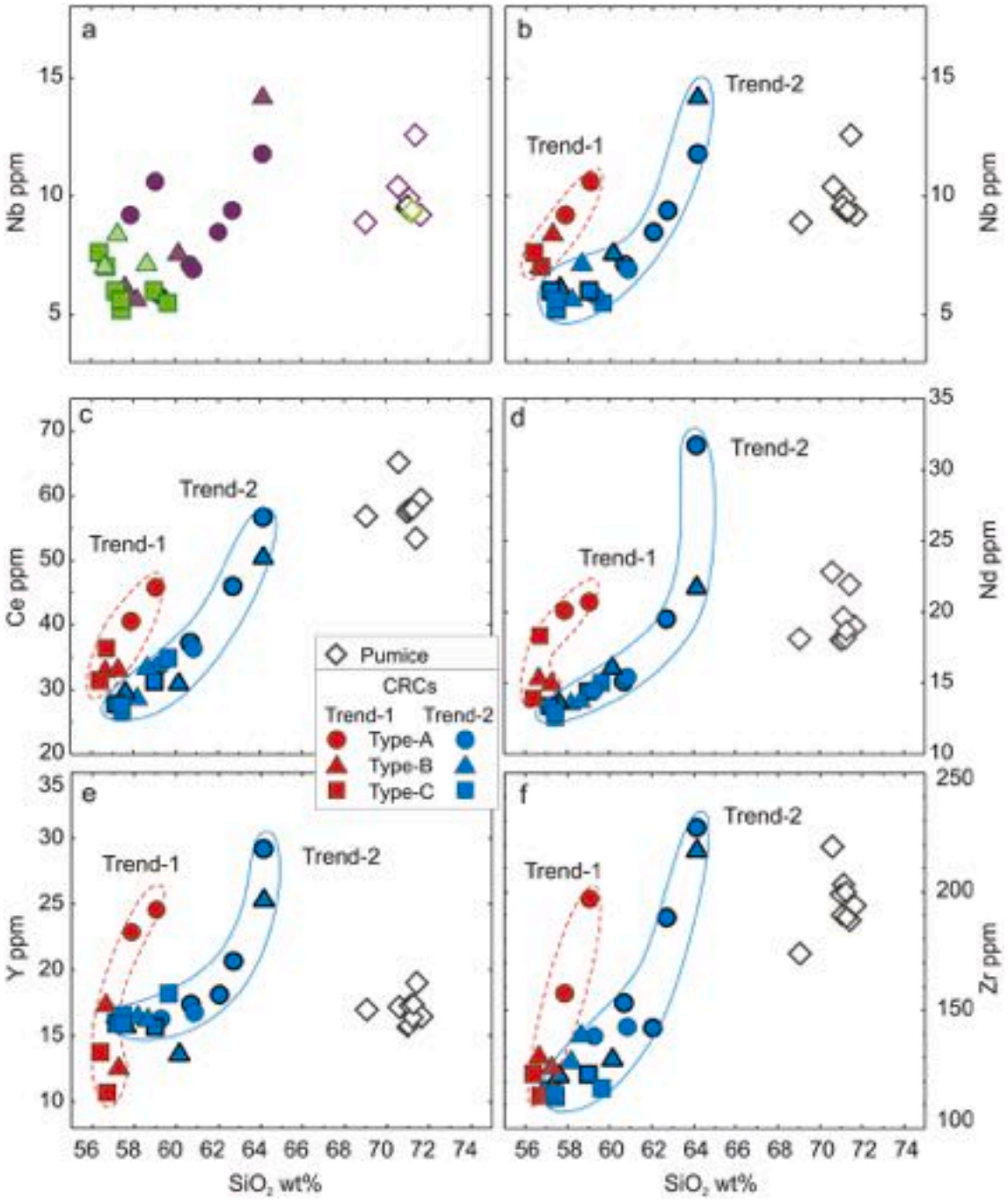

Fig. 8. Variation diagrams of representative incompatible trace elements (ppm) versus silica for the UP pumice and CRC samples. The colour of CRCs symbols hereafter changes to highlight the two compositional groups identified on the basis of geochemical behaviour (Trend-1 and Trend-2, red-dashed and continuous-blue lines, respectively) (b-f) instead of the previous stratigraphic discrimination (a, symbols and colours as in Fig. 6). Symbols still indicate texture types (see legend and text for detail). Symbols with bold, black rim discriminate a further group of samples (namely the sub-trend-2) identified on isotope basis (see text for detail). a) and b) show the same plot (Nb vs silica) to directly compare the two different discriminations of the CRC samples. (For interpretation of the references to colour in this figure legend, the reader is referred to the web version of this article.)

processes are involved. Particularly, $^{143}Nd/^{144}Nd$ and $^{87}Sr/^{86}Sr$ of Trend-2 encompass the whole isotopic range of the CRCs. $^{143}Nd/^{144}Nd$ values are unrelated to silica and incompatible trace element variations (Fig. 10), changing at most among the most mafic products, whereas they seem to remain nearly constant during magma evolution (Figs. 10, 11). On the contrary, $^{87}Sr/^{86}Sr$ values vary among the less evolved magmas and even more during magma evolution, being positively correlated with silica and incompatible trace elements (Figs. 10, 11).

Notably, the observed elemental and isotopic variations of CRCs are correlated with the texture types, and consequently, with the depositional unit. Indeed, the Type-A samples (typical of the fallout deposits) are variable in composition and also showing the highest degree of evolution, whereas the Type-C samples (typical of the lag-breccia deposit) are less evolved and have a lower compositional variation than Type-A, except for Nd-isotopes. The Type-B samples (present in all depositional units) record the largest range of evolutionary degree and encompass the geochemical behaviour of both Type-A and Type-C. No correlation is observed between the composition of the fallout CRCs and

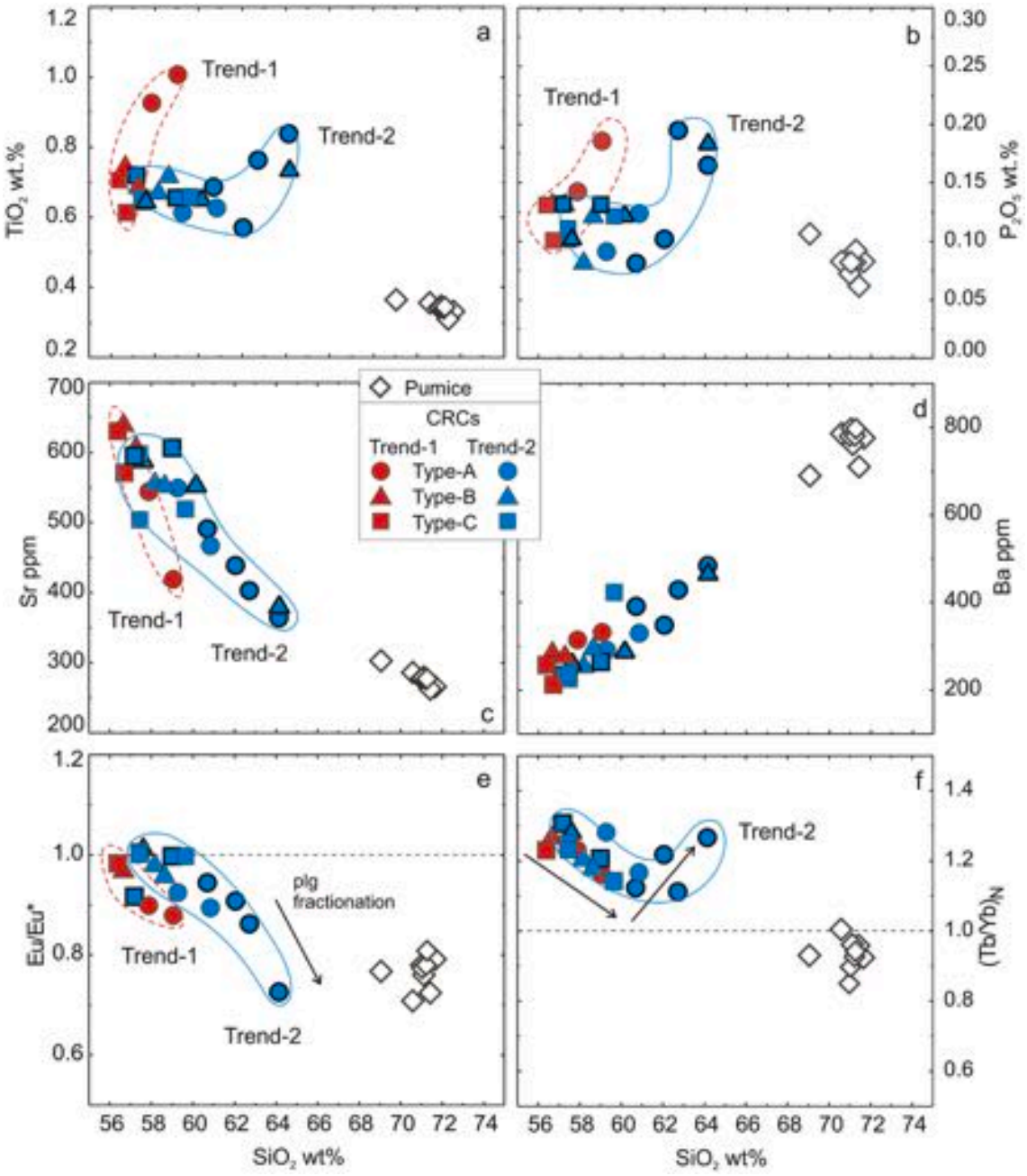

Fig. 9. Variation diagrams of representative minor (a, b; on water free-basis) and trace elements (ppm) (b, c) and chondrite-normalized Tb_N/Yb_N and Eu/Eu* (e, f) versus silica for the UP pumice and CRC samples. Symbols and colours follow the same rationale of Fig. 8.

their outcrop locality, indicating a homogenous distribution of the juvenile products both in the proximal and distal fallout deposits.

5. Discussion

Our data have revealed a large compositional variability within the UP juveniles. A clear distinction particularly exists between pumices, representing the most voluminous rhyolitic magma, and the CRCs, representing more mafic melts (mainly andesites) (Figs. 6-10). Indeed, the textural characteristics of CRCs and their sharp and convolute contacts with pumices suggest they generated from mafic blobs of refilling hot magma that intruded and dispersed into the rhyolitic melt before the eruption, forming magmatic enclaves. The rapid crystallisation induced by the undercooling due to the temperature contrast with the cooler host, prevents their homogenization, and chemical interaction with the rhyolite, preserving their original chemical fingerprint.

The evolved compositions of the CRC matrix glasses, together with the large compositional ranges of the mineral phases, are the result of massive in-situ crystallisation during the rapid undercooling (see also Supplementary Material for further discussions). Notwithstanding their high crystal content, it is unlikely they derived by melting of the crystal-rich fraction of a mush linked to the rhyolitic magma. This is due to: i) the small size of the CRC forming crystals; ii) the different mineral assemblages between pumice and mafic clasts (Fig. 4); iii) the heterogeneous Sr-Nd isotopes values of CRCs compared with the little variability of rhyolitic pumices; iv) the diktytaxitic texture of Type-C clasts; v) the lack of Eu/Eu* values >1, as expected to be found by melting of plagioclase cumulus, and vi) the positive correlation between negative Eu anomalies and silica content in both Trend-1 and Trend-2 (Fig. 9e). Accordingly, the textural characteristics of the different CRC types are

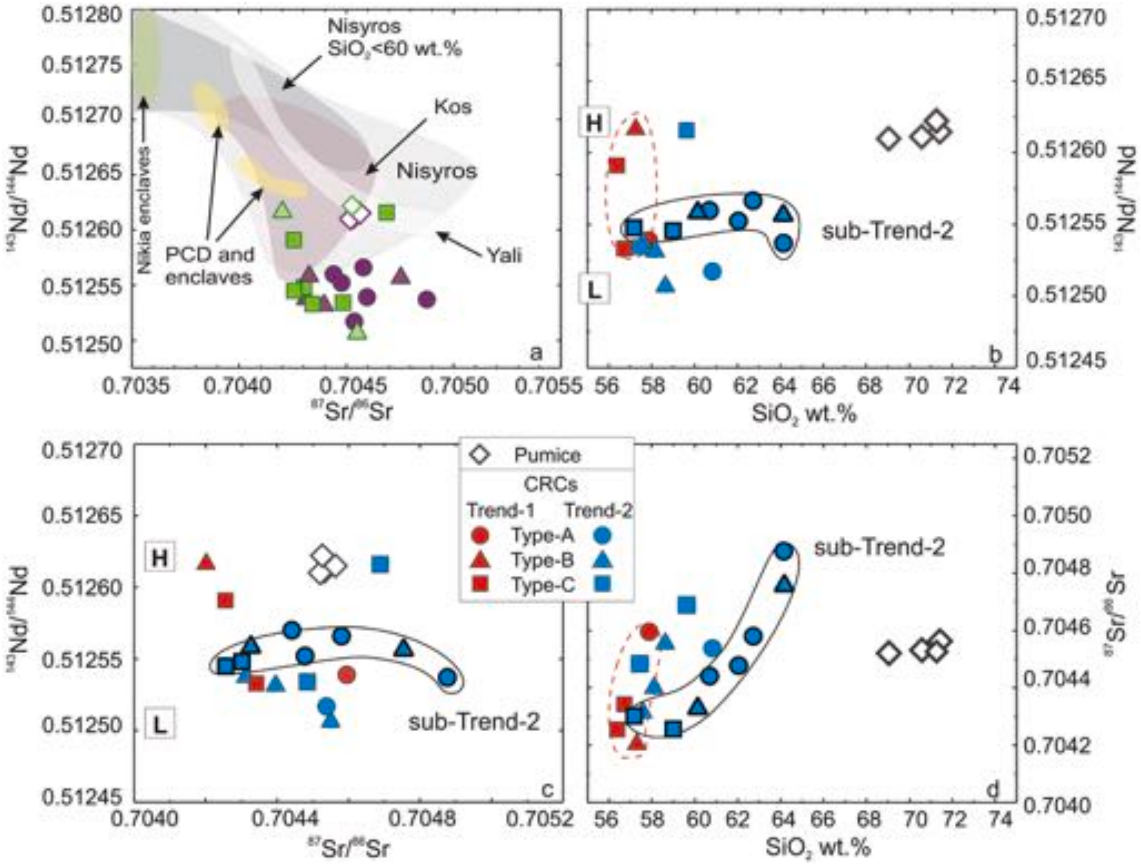

Fig. 10. Variation diagrams of Sr-Nd isotope ratios measured on selected UP samples. (a) $^{87}Sr/^{86}Sr$ versus $^{143}Nd/^{144}Nd$: symbols and colours are the same of Figs. 6 and 7 to show the isotopic variations based on the sample stratigraphic position; shaded fields report for comparison the isotopic variation of available literature data from the Kos-Yali-Nisyros volcanic products (Francalanci et al., 1995; Buettner et al., 2005; Klaver et al., 2018; Bachmann et al., 2007). (b,d) $^{143}Nd/^{144}Nd$ and $^{87}Sr/^{86}Sr$ versus SiO_2, respectively. Labels H and L indicate the High-Nd and Low-Nd isotope values, respectively. (c) $^{87}Sr/^{86}Sr$ versus $^{143}Nd/^{144}Nd$. The red-dashed and the continuous black lines enclose the distribution of Trend-1 and sub-Trend-2 (also defined by symbols with bold, black rim), respectively. (For interpretation of the references to colour in this figure legend, the reader is referred to the web version of this article.)

mainly acquired within the evolved and cooler host magma (see paragraph 5.3), implying that different magmas were contemporaneously present in the UP feeding reservoir at the time of the eruption. The observed correlation between the different types of CRC textures and their stratigraphic position (Figs. 7, 8) implies the presence of a systematic distribution of the different mafic blobs inside the evolved magma reservoir prior the eruption.

The interaction processes between the refilling mafic and host rhyolitic melts, together with the geochemical variations of CRCs, will be discussed in detail in the following paragraphs.

5.1. *The host rhyolitic magma reservoir*

Petrographic, geochemical and isotopic data on pumices suggest that the host rhyolitic magma feeding the UP eruption was essentially homogeneous. The small variations in Al_2O_3, P_2O_5, Sr, Nb, Zr and light REEs within pumices (Figs. 7, 8) reveal a slight compositional zoning of the host evolved magma, ascribed to crystal fractionation of mainly plagioclase, opaques, apatite and zircon.

Pumices contain lots of very small crystal-rich portions (micro-enclaves, Fig. 5), particularly evident in the sample with the lowest silica content (Fig. 6) and probably responsible for its slightly less evolved composition. Despite the presence of micro-enclaves derived from the CRCs, mixing interaction with the mafic melts is excluded because it is not consistent with the observed inter-elemental correlations, especially for some trace elements (e.g., Zr, Y, Nb, REE) and Sr-Nd isotopes (Figs. 8-10). The sharp contact between the CRCs and pumices also rules out the occurrence of mixing (Figs. 3, 5).

This rhyolitic magma was stored in a relatively shallow reservoir with estimated depth of 6–9 or 7–10 km, according to Bachman et al. (2012) and Klaver et al. (2017), respectively. This reservoir probably represents the same magma chamber characterising the entire caldera-forming period of Nisyros, from Lower Pumice to Post-Caldera Domes (i.e., Bachman et al., 2012; Braschi et al., 2012, 2014; Francalanci et al., 1995; Klaver et al., 2017).

5.2. *Differentiation of the mafic Crystal Rich Clast (CRC) magmas*

The largely variable chemical composition of the CRCs suggests the occurrence of complex pre-eruptive evolutionary processes and a composite plumbing system linked to the UP eruption. This assumption is enhanced by the evidence that these different magmas are coeval, being emplaced from a single eruptive event. As previously stated, we exclude significant chemical interaction between the mafic and host evolved melts, implying that the geochemical variability of the CRC mafic magmas must be acquired before their intrusion into the cooler and more evolved host. At this stage, their only mineral cargo should be constituted by few phenocrysts of plagioclase, pyroxene and amphibole.

The general correlations of silica with most of the major and compatible trace elements among the CRC samples (Figs. 6, 7) indicate that crystal fractionation is a leading evolutionary process affecting these magmas.

Trace elements such as REEs and HFSEs, together with TiO_2, P_2O_5 and Na_2O, however, define two parallel trends of positive correlation

with silica (Trend-1 and Trend-2; Figs. 8, 9), suggesting that magma evolution possibly occurred in separate (at least two) magma reservoirs. In both trends, the rapid increase of the above-mentioned elements with differentiation is difficult to attain by a crystal fractionation process alone, unless considering high percentages of crystal fractionation (>60–70%). This is not consistent with their moderate range of silica content, thus requiring the occurrence of other processes.

The complexity of the magma evolution is further highlighted by Sr-Nd isotopes, which are significantly variable and do not correlate to each other (Figs. 10, 11). This is difficult to explain by source heterogeneity because it seems unlikely that coeval magma inputs are not cogenetic. Moreover, to produce the observed variability would need a very heterogeneous mantle source (in space and/or time) and this is not yet demonstrated for the Nisyros volcanic system (Francalanci and Zellmer, 2019). In addition, the Nd-isotopes of CRCs show an anomalously low composition, being the lowest of the Nisyros-Kos-Yali volcanic field (Fig. 10a). At the same time, the relatively high silica content (56–57 wt %) and low Mg# (0.46–0.48) of the less evolved magmas indicate that they had already fractionated to some degree at some level during their ascent through the crust. The observed isotopic variability can be thus better explained by the involvement of crustal Assimilation, associated to Fractional Crystallisation (AFC), as indicated by the general positive correlation between $^{87}Sr/^{86}Sr$ and the evolutionary degree (Fig. 10d). Previous studies have already recognised the role of crustal assimilation in the magma differentiation at Nisyros, even occurring at variable storage depths (Francalanci et al., 1995; Klaver et al., 2017, 2018; Spandler et al., 2012).

The $^{143}Nd/^{144}Nd$ and $^{87}Sr/^{86}Sr$ variations in Trend-1 and Trend-2, moreover, suggest the occurrence of two main evolutionary pathways possibly involving the contribution of distinct crustal components (Figs. 10, 11). The process affecting the most primitive magmas of both Trend-1 and Trend-2 produced a negative Sr-Nd isotope correlation (Fig. 10c), and implies a crustal contaminant able to significantly decrease the $^{143}Nd/^{144}Nd$ values with no or negligible effect on Sr-isotopes. Contrarily, the process occurring from the mafic to more evolved magmas, results in nearly constant Nd-isotopes with considerable increase of $^{87}Sr/^{86}Sr$ and incompatible trace elements (Figs. 10, 11), thus involving a contaminant with comparable $^{143}Nd/^{144}Nd$ and highly radiogenic Sr-isotopes. Furthermore, the coeval presence of all the CRC forming-magmas in a single eruptive event would be difficult to reconcile through AFC processes occurring in a single magma reservoir sited at a fixed crustal level and affected by the same crustal contaminant. Accordingly, we suggest that the evolutionary process affecting the most mafic CRC melts could have occurred at higher depth than the AFC process affecting the other more evolved magmas (Figs. 10, 11). We can realistically suppose that the most primitive CRC melts, after acquiring their variable Nd-isotope ratios at deeper levels, were stored in shallower reservoirs evolving and assimilating a different crustal contaminant. The nature and composition of the possible crustal end-members assimilated by the CRC magmas are reported in Supplementary Material based on the current knowledge of the Aegean and Nisyros basement. The latter can be considered the same as outcropping in Santorini, constituted by Mesozoic limestone and metapelitic/calc-silicate rocks of the Tripolitza Unit, overlying a pre-Alpine orthogneisses crystalline basement. In the proposed model these components represent the more feasible crustal contaminants involved in the AFC process.

5.2.1. The CRC magma evolution by AFC processes at shallow depth

Within both Trend-1 and Trend-2, the $^{87}Sr/^{86}Sr$ values show good general correlation with major and trace elements, whereas $^{143}Nd/^{144}Nd$ values seem not correlated with the other elements (Figs. 10, 11). Based on Nd-isotope variability we observe that the samples distribute at high, intermediate and low $^{143}Nd/^{144}Nd$ values (Figs. 10b,c, 11a,b). Within the intermediate ones, we identify a further sub-trend defined by most of the samples belonging to the Trend-2 (sky-blue symbols with thick-edge in Fig. 10b,c,d). This sub-trend (hereafter sub-Trend-2) includes the most evolved CRC samples and is characterised by a significant Sr-isotope increase with magma evolution, coupled with a good positive correlation of $^{87}Sr/^{86}Sr$ with incompatible trace elements (Figs. 10d, 11d-f). Moreover, looking in detail at the geochemical variation along this sub-trend, the steep increase of $^{87}Sr/^{86}Sr$, REE, HFSE, TiO_2 and P_2O_5 in the most evolved samples (from SiO_2 62 wt%), along with a slight decrease in $^{143}Nd/^{144}Nd$ (Figs. 8, 9, 10b,c,d, 11a,b,c) are remarkable.

We interpret the sub-Trend-2 using quantitative modelling (EC-AFC algorithm; Spera and Bohrson, 2001), aiming to propose a comprehensive interpretation for the compositional characteristics of the CRC samples, including Trend-1 and Trend-2.

The variation of trace elements and radiogenic isotopes along the sub-Trend2 cannot be explained with a single process but requires the involvement of different components. A crustal contaminant like a limestone from the Mesozoic basement, with very low Nd content and relatively high Sr and Sr-isotopes (e.g., Cullers, 2002), could be able to increase the Sr-isotopes without significantly changing the Nd-isotopes. Small carbonate shards dispersed into some CRCs of Type-A and Type-B, could also corroborate this hypothesis. However, EC-AFC quantitative modelling shows that, even considering a few Nd ppm in the contaminant, the Nd-isotope variations in the first part of the sub-Trend-2 cannot be reproduced if the $^{143}Nd/^{144}Nd$ of the crustal component is as low as that of the Tripolitza Unit calc-silicate rocks (0.51221–0.51239, Fig. S3), (Druitt et al., 1999; Klaver et al., 2018). This leads us to invoke for a contaminant with significantly more radiogenic Nd-isotope composition.

Moreover, the assimilation of a pure limestone cannot explain the excessive increase in HFSE and REE (including Nd) observed during the CRC magma evolution (Figs. 8, 9) because carbonate rocks have negligible abundances in all these elements and, as previously stated, crystal fractionation alone is not able to explain their enrichments along Trend-1 and Trend-2. Quantitative calculations suggest that a contaminant enriched in Nd and characterised by high $^{143}Nd/^{144}Nd$ composition, which should be nearly similar to that of the assimilating magma, is required. According to the potential contaminants for the Nisyros magmas described in Supplementary Material, the crustal component suitable for the AFC process of sub-Trend-2 could be that reported by Druitt et al. (1999) from the Santorini basement, with $^{143}Nd/^{144}Nd$ of 0.51260 classified as a marble. Such component would also explain the feeble increase of Nd-isotope along the first part of sub-Trend-2 (Figs. 10b,c, 11a,b).

Furthermore, REEs, HFSEs, TiO_2, P_2O_5, coupled with $^{87}Sr/^{86}Sr$ show a concordant behaviour along the sub-Trend-2, with a marked increase in the most evolved samples (together with a slight $^{143}Nd/^{144}Nd$ decrease; Figs. 8, 9, 10d, 11c-f). This suggests that only these latter melts assimilated a component particularly enriched in those elements, implying a change in the contaminant composition during magma evolution and thus leading to infer the occurrence of a notable heterogeneity in the country rocks. Accordingly, we propose the involvement of carbonate-derived skarn component, possibly occurring as veins or lenses generated by previous magmatic fluid circulations in the wall-rocks. Besides the typical mineral assemblages, such as wollastonite, olivine, pyroxene and plagioclase, these skarn lenses could contain variable amount of garnet, apatite, zircon, epidote and magnetite enriched in HFSEs, REEs, TiO_2 and P_2O_5 (e.g., Ganino et al., 2013; Shu and Liu, 2019; Jiaa et al., 2020). These skarn minerals could have been selectively assimilated by the most evolved CRC magmas, probably during the early magma upward migration, before intruding into the rhyolitic reservoir. This hypothesis could also explain the increase of Tb_N/Yb_N in the CRC samples with silica >62 wt% of the sub-Trend-2 (Fig. 9f), due to the possible digestion of hydrothermal apatite. The assimilation of carbonate-derived skarn was previously proposed for the evolution of the old basaltic-andesite pillows at Nisyros by Spandler et al. (2012), which showed that this process is able to increase the HFSE and REE abundances in the magma.

We quantified the sub-Trend-2 magma evolution by a two-step AFC process, applying the EC-AFC algorithm of Spera and Bohrson (2001) and using two different contaminants for the first ($SiO_2 < 62$ wt%: sub-Trend-2a) and the second step ($SiO_2 > 62$ wt%: sub-Trend-2b). This modelling was validated on $^{87}Sr/^{86}Sr$ and $^{143}Nd/^{144}Nd$ compared to selected key trace elements (blue lines in Fig. 11). The calculated lines of magma evolution well fit the observed sample distribution. The sub-Trend-2a starts from a magma composition similar to that of the less evolved and less Sr-radiogenic sample (NIS416, Table-DB 1) involving the assimilation of a carbonate-rock with Sr-Nd isotopes similar to that of Santorini marble (Druitt et al., 1999) (Fig. 12) and relatively enriched in trace elements (Table 1). The EC-AFC process entails that during the initial, fractionation-dominated stage, the magma intrusion provided the heat to trigger the partial melting of the wallrock. At this moment, the melt isotope signature remains relatively unaltered (Fig. 11). As the process proceeds, the released heat of crystallisation allows the beginning of assimilation and the magma gradually changes its isotopic signature, increasing significantly the $^{87}Sr/^{86}Sr$ and slightly the $^{143}Nd/^{144}Nd$ values (Fig. 11a,b,c). When the sub-Trend-2 changes its slope the calculated mass of crystallised magma (Mc) is 32% of the initial mass, with an amount of crustal assimilation (Ma) of 5%. At this point, the second step of the AFC process (Sub-trend-2b) begins involving a different contaminant, constituted by an enriched skarn component, probably characterised by slightly different Sr-Nd isotopes (Table 1). This induced the rapid increase of $^{87}Sr/^{86}Sr$ and incompatible trace element content, together with a slight $^{143}Nd/^{144}Nd$ decrease encompassing the whole observed variation with maximum Mc = 32% and Ma = 8% (Fig. 11).

The feasibility of this two-step assimilation process relies on the high heat flow characterising the area (e.g., Lucazeau, 2019) and, possibly to repeated arrivals of small, hotter and less fractionated magma inputs, which refill the reservoir and provide the sufficient thermal energy to promote a progressive assimilation. These multiple batches can be inferred by the emplacement sequence of the different CRCs (see next paragraph 5.3).

The processes proposed for the sub-Trend-2 evolution can be reasonably extended to account for the different CRC compositions that deviate from it in both Trend-1 and Trend-2 (Fig. 10b-d). We can hypothesise that similar shallow level processes increased the $^{87}Sr/^{86}Sr$ at nearly constant $^{143}Nd/^{144}Nd$, starting from primitive magmas with different Nd-isotopes (horizontal blue arrows in Fig. 11a). Moreover, a few CRC samples of Trend-2 show particularly low incompatible trace element contents associated with relatively high $^{87}Sr/^{86}Sr$ (Figs. 10, 11). Three of these samples (dotted field in Fig. 11) belong to the

Table 1
EC-AFC parameters used for the simulation of the two shallow and deep processes involving the CRCs forming melts. Details are provided in Supplementary Material.

Two-steps shallow process								
a								
Step1: sub-Trend-2a								
Thermal parameter			Compositional parameter					
tlm	1130	degC	Element	Sr	Nd	Ce	Zr	Nb
tm0	1130	degC		ppm	ppm	ppm	ppm	ppm
tla	1100	degC	Magma	660	12	27	110	5
ta0	300	degC	bulk D0	2.2	0.1	0.1	0.1	0.1
ts	800	degC						
cpm	1484	J/kg K	Contaminant	400	18	15	40	9
cpa	1410	J/kg K	bulk D0	1	1	1	1	1
hcry	396,000	J/kg						
hfus	250,000	J/kg	Isotope	$^{87}Sr/^{86}Sr$	$^{143}Nd/^{144}Nd$			
Teq	998	degC	Magma	0.70427	0.51255			
			Contaminant	0.70800	0.51260			
b								
Step2: sub-Trend-2b								
Thermal parameter			Compositional parameter					
tlm	1120	degC	Element	Sr	Nd	Ce	Zr	Nb
tm0	1120	degC		ppm	ppm	ppm	ppm	ppm
tla	1000	degC	Magma	550	16.5	33	133	6.5
ta0	300	degC	bulk D0	2.1	0.1	0.1	0.1	0.1
ts	800	degC						
cpm	1484	J/kg K	Contaminant	320	50	125	530	35
cpa	1410	J/kg K	bulk D0	1	1	1	1	1
hcry	396,000	J/kg						
hfus	250,000	J/kg	Isotope	$^{87}Sr/^{86}Sr$	$^{143}Nd/^{144}Nd$			
Teq	990	degC	Magma	0.70447	0.51256			
			Contaminant	0.71000	0.51248			
c								
Deep process								
Thermal parameter			Compositional parameter					
tlm	1150	degC	Element	Sr	Nd			
tm0	1150	degC		ppm	ppm			
tla	1090	degC	Magma	660	12.5			
ta0	420	degC	bulk D0	1.6	1			
ts	800	degC						
cpm	1484	J/kg K	Contaminant	50	13			
cpa	1370	J/kg K	bulk D0	0.7	0.1			
hcry	396,000	J/kg						
hfus	270,000	J/kg	Isotope	$^{87}Sr/^{86}Sr$	$^{143}Nd/^{144}Nd$			
Teq	1020	degC	Magma	0.70419	0.51262			
			Contaminant	0.74000	0.51190			

Footnotes: tlm = magma liquidus temperature; tm0 = initial magma temperature; tla = wallrock liquidus temperature; ta0 = initial wallrock temperature; ts = solidus temperature; cpm = isobaric specific heat of magma; cpa = isobaric specific heat of assimilant; hcry = crystallisation enthalpy; hfus = fusion enthalpy; Teq = equilibrium temperature.

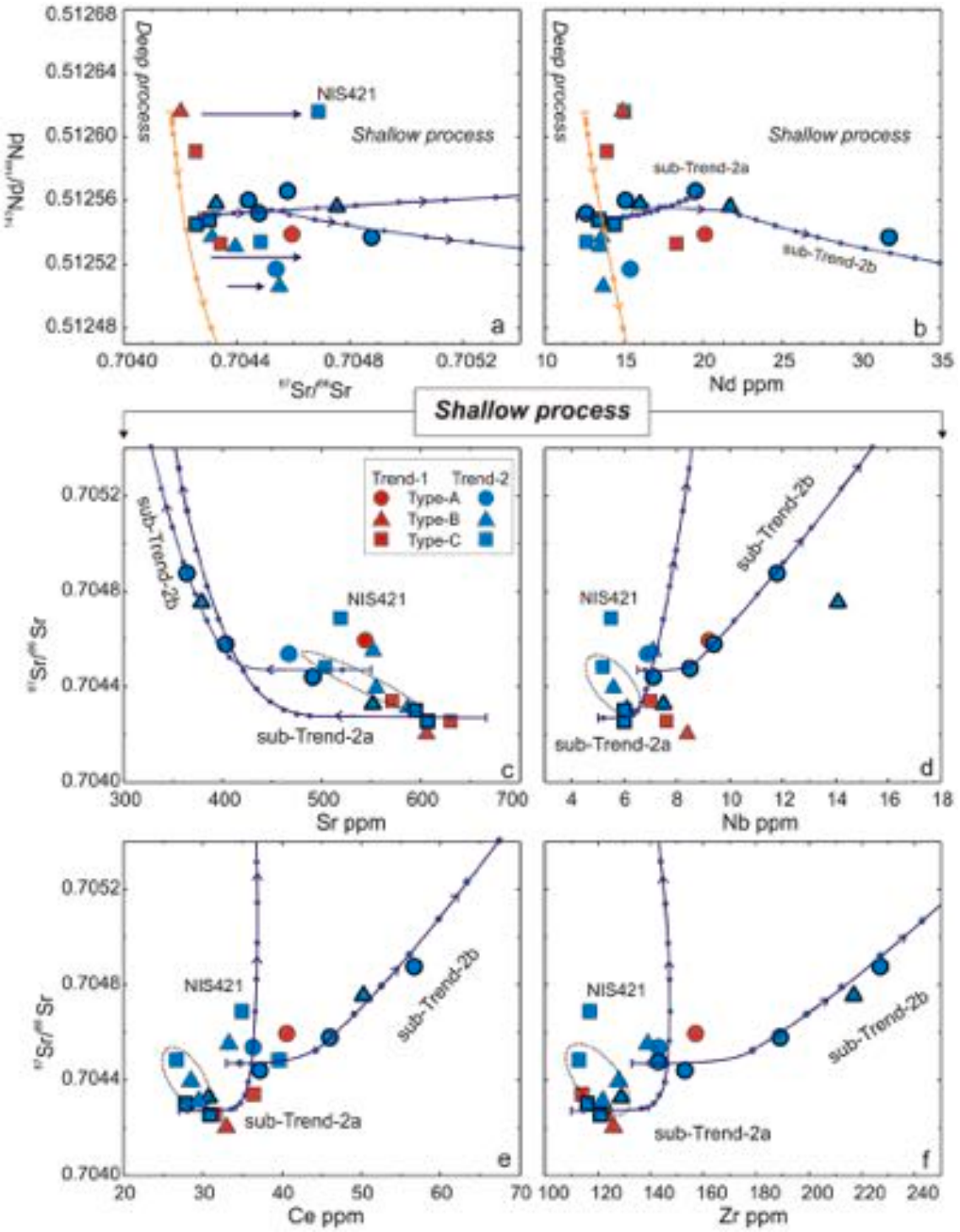

Fig. 11. Sr-Nd isotope ratios versus selected key trace elements showing the results of the EC-AFC simulations for the CRC magma evolution following the model of Spera and Bohrson (2001). (a) $^{87}Sr/^{86}Sr$ versus $^{143}Nd/^{144}Nd$; (b) $^{143}Nd/^{144}Nd$ versus Nd (ppm); (c-f) $^{87}Sr/^{86}Sr$ versus Sr, Nb, Ce, Zr (ppm). Dotted field includes the three samples with intermediate $^{143}Nd/^{144}Nd$ characterised by low incompatible trace element contents prone to pure limestone contamination. Blue lines represent the modelling of the two-step shallow process described by sub-Trend-2a and sub-Trend-2b. The orange line (in plot a and b) models the deep process involving the most mafic magmas and encompassing the whole Nd-isotope variability. Arrows indicate the direction of falling magma temperature (Tm) along the model. Each dot on EC-AFC curves represents a normalized temperature decrease of 0.002 (3 °C). Thermal parameters and input compositions used in the models are reported in Table 1 and detailed in Supplementary Material. (For interpretation of the references to colour in this figure legend, the reader is referred to the web version of this article.)

intermediate $^{143}Nd/^{144}Nd$ (SiO_2 around 58 wt%), whereas the fourth sample (NIS421, Type-C) displays the highest $^{143}Nd/^{144}Nd$ value recorded within the Trend-2 (Fig. 10b,c). The latter is also the most evolved (SiO_2 59.5 wt%) and the most radiogenic in $^{87}Sr/^{86}Sr$ among the lag-breccia CRCs (Figs. 10, 11). These geochemical features require the involvement of another crustal contaminant depleted in trace elements, such as a relatively pure limestone/marble, thus further supporting the presence of heterogeneous, carbonate-type basement.

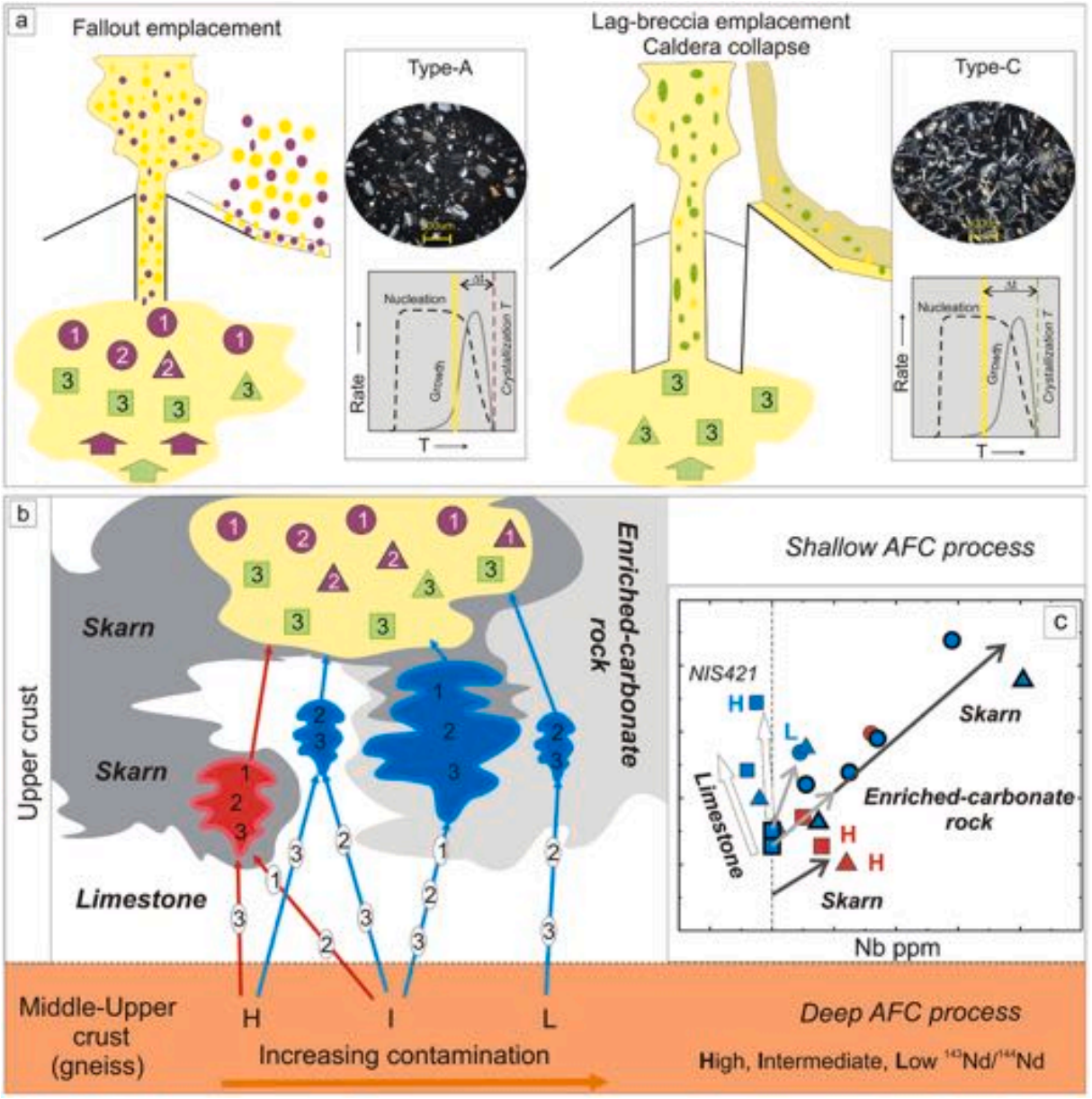

Fig. 12. Schematic cartoons summarizing the inferred setting of the rhyolitic magma chamber during the two main phases of the UP eruption (a) and the possible scenario of ascent, transient crustal storage, crystallisation and assimilation of the CRCs forming magmas at different depth (red and sky-blue reservoirs for the shallow process of Trend-1 and Trend-2, respectively and orange field for the deeper process), together with their dynamics of progressive batch intrusion in the rhyolitic reservoir (yellow) (b). Red and sky-blue pockets indicate distinct reservoirs assimilating different type of wallrocks (limestone, enriched-metasomatised carbonates and skarn). The largest sky-blue reservoir hosts the sub-Trend-2 evolution (2a: assimilation of relatively enriched carbonate-rocks at the bottom; 2b: assimilation of enriched skarn at the top). Encircled numbers indicate the ascent progression of the different magma batches and their distribution as enclaves in the shallow magma chamber. The inset (c) show the Nb versus $^{87}Sr/^{86}Sr$ behaviour recalling the compositional variations induced by assimilation of the different wallrocks (white to dark grey). Bold white arrows indicate the effect of limestone assimilation; grey and black arrows indicate the effect of enriched-carbonate and skarn assimilation, respectively. The two insets in (a) illustrate the formation of the different CRC texture types according to variable undercooling conditions (**Δt**) due to their different crystallisation temperatures in the cooler host magma (yellow line). (For interpretation of the references to colour in this figure legend, the reader is referred to the web version of this article.)

Furthermore, considering that along the Trend-1, including the least evolved samples, REEs and HFSEs are more enriched than in Trend-2, we suggest that they evolved in a separate reservoir formed in a skarn-enriched zone of the country rocks. In this light, the lowest $^{87}Sr/^{86}Sr$ values of the Trend-1 mafic samples may look contrasting. However, nothing prevents that the original magmas had even less radiogenic $^{87}Sr/^{86}Sr$ that was successively increased by the skarn assimilation, together with trace element contents. Besides, comparing the most mafic samples of the two trends, the lower Y, MgO and slightly higher Al_2O_3 and Sr contents of the Trend-1 (Figs. 7-9), suggests different crystallisation conditions (possibly higher pressure), where amphibole is favoured in respect to plagioclase. The proceeding of assimilation of a trace element-enriched skarn component led anyway to highly increase the Y contents.

The need of contaminant end-members with relatively high $^{143}Nd/^{144}Nd$ values, similar to those of the assimilating magmas, could be a critical point of this model, considering that only one sample with this peculiar characteristic is available, and belongs to the Santorini basement (Druitt et al., 1999). However, we can interpret that the required specific Nd-isotope composition may be acquired by these

carbonate and skarn contaminants through earlier magmatic fluid circulations that might have metasomatised the original rocks and imprinted their $^{143}Nd/^{144}Nd$ signature. This might be reasonable considering that values around 0.5126 are measured in several volcanic products from the past activity of Kos, Yali and Nisyros, also including the UP rhyolitic pumices (Figs. 10a, 12). The significantly low Nd contents, compared to Sr, of carbonate rocks (e.g., Cullers, 2002) could be the reason for the efficient magmatic imprinting of the Nd- rather than Sr-isotopes. The relatively high $^{143}Nd/^{144}Nd$ signature of the suitable contaminant, associated with the incompatible trace element enrichment, could also indicate interaction with interstitial melts from crystal mushes, whose presence has been suggested for many volcanoes in literature (e.g., Cashman et al., 2017) including the Kos-Nisyros-Yali system (Bachman et al., 2012; Popa et al., 2019). However, we exclude this hypothesis because: i) it is realistically difficult to assimilate only interstitial melts; ii) such assimilation would have particularly increased the silica content besides trace elements (matrix glasses have SiO_2 content up to 78 wt%), contrarily to what we observe in the sub-Trend-2b (Figs. 8, 9); iii) $^{87}Sr/^{86}Sr$ would have not increased.

Finally, the presence of carbonate-rocks below the bottom of the magma chamber could be a critical point considering the inferred depth for the Nisyros rhyolitic magma chamber (i.e., 4–10 km, Bachman et al., 2012; Klaver et al., 2018, Popa et al., 2019). However, the important thickness of the carbonate Mesozoic basement (up to 3 km), the presence of an intense tectonic control on volcanic structures in this area (Papazachos and Panagiotopoulos, 1993; Tibaldi et al., 2008), together with the multiple caldera collapse events that affected the Kos-Nisyros volcanic field, leads us to interpret the possible presence of carbonate basement even at relatively deep levels in the upper crust.

5.2.2. *The AFC differentiation process of the mafic CRC magmas at depth*

The most primitive CRC samples form a negative Sr-Nd isotope correlation with a significant decrease in Nd-isotopes associated with a small increase in Sr-isotopes (Fig. 10a-c), suggesting the involvement of a crustal component with particularly low $^{143}Nd/^{144}Nd$, opposite to those involved at shallow level, as previously discussed. These isotopic variations do not significantly correlate with the incompatible trace element contents, due to the effect of the successive shallow AFC processes, which also affected trace element abundances of most CRCs. This makes it difficult to infer the possible geochemical composition and nature of this crustal contaminant.

The andesitic composition (SiO_2 56–57 wt%, Mg# 0.46–0.48) of the less evolved magmas leads us to exclude an AFC process in the lower-crust, which would provide the suitable low $^{87}Sr/^{86}Sr$ and $^{143}Nd/^{144}Nd$ composition, because an intermediate magma would not be able to assimilate such mafic components. Furthermore, the inferred lower-crust composition below Nisyros suggested by Buettner et al. (2005) or Klaver et al. (2018) has an isotopic signature that seems not suitable for this AFC process (Fig. S3).

We quantified the Sr-Nd isotope variation of the least evolved magmas applying the EC-AFC algorithm of Spera and Bohrson (2001), assuming a single process occurring at depth. For this model we select a contaminant similar to the pre-alpine basement (i.e., a gneiss outcropping in Ios island, Buettner et al., 2005 and Klaver et al., 2018) representative of a middle-crust with low $^{143}Nd/^{144}Nd$ and high $^{87}Sr/^{86}Sr$ (Fig. S3). Results are shown in Fig. 11a,b and the thermal and compositional input parameters used are reported in Table 1 (see also Supplementary Material). The initial magma composition is similar to the least evolved, least Sr-radiogenic and most Nd-radiogenic sample belonging to the Trend-1. The calculated model reproduces the observed Nd-isotope decrease among the most primitive CRC magmas (orange lines in Fig. 11a,b). It shows a sudden significant $^{143}Nd/^{144}Nd$ decrease after very low degree of fractionation and assimilation, and proceeds further with a small change in $^{87}Sr/^{86}Sr$ values, crossing the magma composition from which the sub-Trend-2 begins. The lowest Nd-isotope values recorded by the CRCs correspond to about 2% of assimilation (Ma), coupled with a maximum fractional crystallisation (Mc) of 18%. This is a reasonable value for magmas that show a silica increase of about 2%. From these results we interpret that a relatively mafic magma was stored at depth in the middle crust, evolving by crystallisation and assimilation of different degrees and thus acquiring variable Nd-isotope signature. Single distinct batches then ascended and experienced the successive evolutionary shallow processes within different magma reservoirs modelled in paragraph 5.1.

5.3. *UP plumbing system dynamics: linking textural, chemical, and stratigraphic data*

The simultaneous presence of geochemically variable melts in the shallow magma chamber feeding the UP eruption, together with the proposed interpretation of the geochemical variability of CRCs, suggest that they represent batches of variably fractionated and contaminated magmas formed within a complex, polybaric plumbing system involving different crustal contaminants (Fig. 12b,c). During the final stage of their ascent to the surface, these magmas progressively intruded and dispersed into the rhyolitic magma of the UP reservoir without mixing with the host melt, thus maintaining their geochemical signatures (Fig. 12a,b).

The correlation between the geochemical and textural characteristic of CRCs and their stratigraphic occurrence in the UP deposit is also of fundamental importance and mark the dynamics of ascent, intrusion and eruption. The Type-A (and some Type-B) are mainly found in the basal fallout deposits, thus implying they are emplaced at the beginning of the eruption. Contrarily, the more mafic Type-C (and the less evolved Type-B), mostly present in the successive lag-breccia deposits, are erupted during the later caldera stage. This suggests a sort of zoning of the different mafic magma batches inside the rhyolitic magma chamber, where the Type-A (and the more evolved Type-B) sited in the upper and central part of the reservoir, whereas the Type-C were located in the lower part (Fig. 12a).

As proposed in paragraph 5.2.1, the Trend-1 and sub-Trend-2 reveal the presence of at least two main magma reservoirs, maybe relatively small in size considering the small volume of the CRC products. We also suggest that the reservoir related to the Trend-1 was possibly entirely sited at slightly higher pressure than those of sub-Trend-2, within a skarn-dominated country rock. The contemporaneous presence of all the CRC melts and their systematic zoning in the UP magma chamber allow supposing that the small CRC shallow reservoirs were in turn compositionally zoned with the more mafic melts at the bottom (Fig. 12). This was possibly due to new, hotter magma re-inputs (sequentially indicated by numbers in Fig. 12b) from the deeper magma storage level (orange field in Fig. 12b) that also supplied the necessary heat for the on-going crustal contamination. The evidence that the lag-breccia CRCs are highly heterogeneous in Nd-isotopes (Fig. 10a) and represent the primitive terms of all the evolutionary trends (Fig. 8a,b) indicates that new magma inputs involved all the different CRC shallow reservoirs, thus implying a dynamic process with frequent uprising of mafic CRC melts, variably contaminated at deeper level.

The evolved melts of the Trend-1 and sub-Trend-2, which include most of the CRCs found in the fallout (Fig. 8a,b), must represent the first batches intruding into the overlying UP rhyolitic magma chamber, where they progressively moved in its upper part (batches 1 in Fig. 12b). Their isotopic signature suggests that the two main CRC shallow reservoirs were initially fed with primitive magmas having intermediate $^{143}Nd/^{144}Nd$ values acquired by AFC processes at higher depth. While in the Trend-1 reservoir (red pocket in Fig. 12b) this magma directly evolved assimilating enriched skarn components, in the sub-Trend-2 reservoir (sky-blue pocket in Fig. 12b) it firstly evolved (up to SiO_2 62 wt%: sub-Trend-2a) assimilating a carbonate-rock relatively enriched in trace elements. The process continued by assimilation of skarn phases possibly diffused in the wallrock above the reservoir, while the magma opened its way upward. Meanwhile these melts evolved and ascended,

new magmas with intermediate and high $^{143}Nd/^{144}Nd$ (H in Fig. 12c, namely the less contaminated in the deep AFC process) progressively refilled the sub-Trend-2 and Trend-1 reservoirs, respectively (batch 2 and 3 in Fig. 12b). The ascent efficiency of the CRC magmas towards and inside the shallow rhyolitic magma chamber was possibly favoured by the CO_2 release from the carbonate-rock reaction during assimilation, likely forming a free vapour phase due to the low CO_2 solubility in arc magmas (Spandler et al., 2012). This gas-vapour phase enrichment could also account for the high vesicle content in the CRC magmas (especially in Type-A and Type-B).

The presence of other smaller volume magma ponding is then hypothesised in order to explain some distinct compositions observed among the CRC samples of the Trend-2, as discussed above. Accordingly, mafic magma batches with intermediate $^{143}Nd/^{144}Nd$ may have raised and rested through a near pure limestone country-rock (small sky-blue reservoir Fig. 12b), whose assimilation would have increased their Sr-isotopes but not the incompatible trace elements (white arrows of Fig. 12c). The same contaminant possibly affected the NIS421-forming melts, originated by mafic magmas with high $^{143}Nd/^{144}Nd$. Finally, mafic melts with lower Nd-isotopes (L in Fig. 12c, namely the more contaminated in the deep AFC process) could have ascended through relatively enriched carbonate-rocks, moderately increasing their incompatible trace elements (grey arrows in Fig. 12c).

The overall correlation between the CRC textures and compositions can be ascribed to their different undercooling conditions inside the cooler rhyolitic host magma. Although all the CRC textures indicate a massive crystallisation with high nucleation and low growth rates, the different crystal habitus, mainly tabular in the Type-A and acicular in the Type-C clasts (Fig. 4, insets in Fig. 12a), suggests slightly higher undercooling conditions in the latter. We can reasonably interpret that the more evolved and carbonate-contaminated Type-A melts have lower crystallisation temperature than that of the Type-C melts, thus inducing a lower undercooling with the host magma temperature (insets in Fig. 12a). Geo-thermometer calculations also confirm higher crystallisation temperatures for Type-C than Type-A melts (e.g., 820–1020 and 780–930 °C respectively, applying the Ridolfi, 2021 geo-thermometer) (Supplementary Materials). Finally, the more variable textures of the Type-B clasts may be the result of variable undercooling as they moved in different portions of the rhyolitic reservoir with slightly different temperature gradients.

The top of the rhyolitic magma chamber hosting the Type-A and Type-B melts fed the beginning of the UP eruption, whereas the bottom of the reservoir including the Type-C mafic blobs was involved in the late caldera phase, leading to the peculiar distribution of the CRC clasts in the UP deposits (Fig. 12a).

6. Conclusions

The combination of stratigraphic, petrographic, geochemical and isotopic studies of the juvenile products of the last explosive magmatic event on Nisyros volcano (Upper Pumice sub-Plinian eruption) allowed us to define a complex magma ponding and crustal assimilation system, mainly linked to the ascent and resting of relatively primitive magma batches before their input into the main rhyolitic reservoir.

This complex plumbing system is revealed by a large heterogeneity of the juveniles, signifying that different magmas were present in the feeding reservoir of the UP eruption. Pumices represent the most voluminous rhyolitic magma, associated with about 10–15 vol% of andesitic (up to few dacitic) melts forming the CRCs by variable undercooling inside the cooler rhyolitic host magma. The CRCs are characterised by three different textures (Type-A, Type-B, Type-C), with specific recurrence in the different depositional units and correlated with their evolutionary degree, whereas isotope ratios show more complex variations.

We identify two distinct AFC processes developed at two different crustal levels, within two different country rocks, that likely account for the observed geochemical and isotopic recurrence of CRCs. A first, relatively deep process occurred within a gneissic basement having low Nd-isotopes, producing the large variation in $^{143}Nd/^{144}Nd$ of the most primitive magmas, coupled with a small change in $^{87}Sr/^{86}Sr$. A shallow process, developed within a heterogeneous and variably enriched carbonate basement with higher $^{143}Nd/^{144}Nd$, occurred within different and relatively small reservoirs, thus justifying the high variability of trace elements and $^{87}Sr/^{86}Sr$ values.

During the shallow process, the involvement of a carbonate contaminant has the potential to generate CO_2 release that could promote the ascent of the different magma batches into the rhyolitic magma chamber, also explaining the high vesicle content of the CRC magmas (especially in Type-A and Type-B) (Blythe et al., 2015). Although the small amount of mafic recharge, the input of CO_2-rich melts could have contributed to generate the necessary overpressure for triggering the UP eruption, discharging a large amount of CO_2 into the atmosphere through the explosive plume. This reconciles with several findings where the involvement of carbonate components and the interaction between magma and the hydrothermal skarn-forming system represents a critical aspect for volcanic behaviour (e.g., Campi Flegrei, Etna, Merapi, Popocatépetl, Somma-Vesuvius; Buono et al., 2020; Chadwick et al., 2007).

The transient character of these CRC magmas is another notable point. They are indeed the only one having such low Nd-isotopes, especially if compared to the Nisyros less evolved magmas and particularly to the mafic melts found as enclaves both in the previously erupted Nikia lavas and in the successively erupted Post-Caldera Domes. It seems that only during the UP pre-eruptive stage, magmas ascended and experienced a significant crustal assimilation, probably favoured by a different tectonic regime.

Declaration of Competing Interest

None.

Acknowledgment

The authors sincerely thank all the researchers associated to the Radiogenic Isotopes Laboratory of Florence and Pisa for assistance during analysis and isotope measurements. Special thanks to Laura Chiarantini for assistance during SEM session and Andrea Orlando for the useful suggestions and discussions. Derek Keir is warmly thanked for the critical review of the English style. The financial support was provided by Italian MIUR through the PRIN-2017 funding grant 20178LPCPW, issued to LF. Insightful comments of two anonymous reviewers helped to significantly improve this manuscript and are acknowledged.

Appendix A. Supplementary data

Supplementary data to this article can be found online at https://doi.org/10.1016/j.lithos.2021.106574.

References

Avanzinelli, R., Boari, E., Conticelli, S., Francalanci, L., Guarnieri, L., Perini, G., Petrone, C.M., Tommasini, S., Ulivi, M., 2005. High precision Sr, Nd, and Pb isotopic analyses using the new generation thermal Ionisation Mass Spectrometer ThermoFinnigan Triton-Ti®. Period. Miner. 74 (3), 147–166.

Bachman, O., Deering, C.D., Ruprecht, J.S., Huber, C., Skopelitis, A., Schnyder, C., 2012. Evolution of silicic magmas in the Kos-Nisyros volcanic center, Greece: a petrological cycle associated with caldera collapse. Contrib. Mineral. Petrol. 163, 151–166. https://doi.org/10.1007/s00410-011-0663-y.

Bachmann, O., Charlier, B.L.A., Lowenstern, J.B., 2007. Zircon crystallization and recycling in the magma chamber of the rhyolitic Kos Plateau Tuff (Aegean arc). Geology 35 (1), 73–76. https://doi.org/10.1130/G23151A.1.

Bacon, C.R., 1986. Magmatic inclusions in silicic and intermediate volcanic rocks. J. Geophys. Res. 91, 6091. https://doi.org/10.1029/JB091iB06p06091.

Barberi, F., Navarro, J.M., Rosi, M., Santacroce, R., Sbrana, A., 1988. Explosive interaction of magma with ground water: insights from xenoliths and geothermal drillings. Rend. Soc. Ital. Mineral. Petrol. 43, 901–926.
Blake, S., 1990. Viscoplastic models of lava domes, in Lava Flows and Domes. In: Fink, J. H. (Ed.), AVCEI Proc Volcan, vol. 2. Springer-Verlag, New York, pp. 88–126.
Blake, S., Fink, J.H., 2000. On the deformation and freezing of enclaves during magma mixing. J. Volcanol. Geotherm. Res. 95, 1–8. https://doi.org/10.1016/S0377-0273(99)00129-8.
Blythe, L.S., Deegan, F.M., Freda, C., Jolis, E.M., Masotta, M., Misiti, V., Taddeucci, J., Troll, V.R., 2015. CO_2 bubble generation and migration during magma–carbonate interaction. Contribution to. Mineral. Petrol. 169, 42. https://doi.org/10.1007/s00410-015-1137-4.
Braschi, E., Francalanci, L., Vougioukalakis, G.E., 2012. Inverse differentiation pathway by multiple mafic magma refilling in the last magmatic activity of Nisyros Volcano, Greece. Bull. Volcanol. 74, 1083–1100. https://doi.org/10.1007/s00445-012-0585-1.
Braschi, E., Francalanci, L., Tommasini, S., Vougioukalakis, G.E., 2014. Unraveling the hidden origin and migration of plagioclase phenocrysts by in situ Sr isotopes: the case of final dome activity at Nisyros volcano, Greece. Contrib. Mineral. Petrol. 167, 988. https://doi.org/10.1007/s00410-014-0988-4.
Buettner, A., Kleinhanns, I.C., Rufer, D., Hunziker, J.C., Villa, I.M., 2005. Magma generation at the easternmost section of the Hellenic arc: Hf, Nd, Pb and Sr isotope geochemistry of Nisyros and Yali volcanoes (Greece). Lithos 83, 29–46. https://doi.org/10.1016/j.lithos.2005.01.001.
Buono, G., Pappalardo, L., Harris, C., Edwards, B.R., Petrosino, P., 2020. Magmatic stoping during the caldera-forming Pomici di Base erutpion (Somma-Vesuvius, Italy) as a fuel of eruption explosivity. Lithos 370–371, 105628. https://doi.org/10.1016/j.lithos.2020.105628.
Caliro, S., Chiodini, G., Galluzzo, D., Granieri, D., La Rocca, M., Saccorotti, G., Ventura, G., 2005. Recent activity of Nisyros volcano (Greece) inferred from structural, geochemical and seismological data. Bull. Volcanol. 67, 358–369. https://doi.org/10.1007/s00445-004-0381-7.
Cashman, K.V., Sparks, R.S.J., Blundy, J.D., 2017. Vertically extensive and unstable magmatic systems: a unified view of igneous processes. Science 355, 6331, eaag3055. https://doi.org/10.1126/science.aag3055.
Chadwick, J.P., Troll, V.R., Ginibre, C., Morgan, D., Gertisser, R., Waight, T.E., Davidson, J.P., 2007. Carbonate Assimilation at Merapi Volcano, Java, Indonesia: insights from crystal isotope stratigraphy. J. Petrol. 48, 1793–1812. https://doi.org/10.1093/petrology/egm038.
Cullers, L.R., 2002. Implications of elemental concentrations for provenance, redox conditions, and metamorphic studies of shales and limestones near Pueblo, CO, USA. Chem. Geol. 191, 305–327.
Davì, M., De Rosa, R., Holtz, F., 2010. Mafic enclaves in the rhyolitic products of Lipari historical eruptions; relationships with the coeval Vulcano magmas (Aeolian Islands, Italy). Bull. Volcanol. 72, 991–1008. https://doi.org/10.1007/s00445-010-0376-5.
Davis, E.N., 1967. Zur Geologie und Petrologie der Inseln Nisyros und Jali (Dodekanes). Praktika Akan Athen 42, 235–252.
Di Salvo, S., Avanzinelli, R., Isaia, R., Zanetti, A., Druitt, T., Francalanci, L., 2020. Crystal-mush reactivation by magma recharge: evidence from the Campanian Ignimbrite activity, Campi Flegrei volcanic field, Italy. Lithos 376–377, 105780. https://doi.org/10.1016/j.lithos.2020.105780.
Druitt, T.H., 2006. New insights into the initiation and venting of the Bronze-Age eruption of Santorini (Greece), from component analysis. Bull. Volcanol. 76, 794. https://doi.org/10.1007/s00445-014-0794-x.
Druitt, T.H., Edwards, L., Mellors, R.M., Pyle, D.M., Sparks, R.S.J., Lanphere, M., Dvies, M., Barreirio, B., 1999. Santorini Volcano, 19. Geological Society London Memoirs.
Forni, F., Bachman, O., Mollo, S., De Astis, G., Gelmand, S.G., Ellisa, B.S., 2016. The origin of a zoned ignimbrite: Insights into the Campanian Ignimbrite magma chamber (Campi Flegrei, Italy). Earth Planet. Sci. Lett. 449, 259–271.
Francalanci, L., Vougioukalakis, G.E., Perini, G., Manetti, P., 2005. A West-East Traverse along the magmatism of the south Aegean volcanic arc in the light of volcanological, chemical and isotope data. Dev. Volcanol. 7, 65–111.
Francalanci, L., Zellmer, G.F., 2019. Magma Genesis at the South Aegean Volcanic Arc. Elements 15, 165–170. https://doi.org/10.2138/gselements.15.3.165.
Francalanci, L., Varekamp, J.C., Vougioukalakis, G., Defant, M.J., Innocenti, F., Manetti, P., 1995. Crystal retention, fractionation and crustal assimilation in a convecting magma chamber, Nisyros Volcano, Greece. Bull. Volcanol. 56, 601–62020.
Francalanci, L., Braschi, E., Di Salvo, S., Lucchi, F., Petrone, C.M., 2014. When magmas do not interact: paired Roman-age activity revealed by tephra studies at Stromboli volcano. Bull. Volcanol. 76, 884. https://doi.org/10.1007/s00445-014-0884-9.
Ganino, C., Harris, C., Arndt, N.T., Prevec, S.A., Howarth, G.H., 2013. Assimilation of carbonate country rock by the parent magma of the Panzhihua Fe-Ti-V deposit (SW China): evidence from stable isotopes. Geosci. Front. 4, 547–554. https://doi.org/10.1016/j.gsf.2012.12.006.
Gansecki, C., 1991. Petrology of the Domes and Inclusions of Nisyros Volcano, Dodecanese Islands, Greece. Bachelor Thesis. Wesleyan University, Middletown, Connecticut, p. 97.
Hardiman, J.C., 1999. Deep sea tephra from Nisyros Island, eastern Aegean Sea, Greece. Geol. Soc. Lond. Spec. Publ. 161, 69–88. https://doi.org/10.1144/GSL.SP.1999.161.01.06.
Jiaa, F., Zhanga, C., Liu, H., Mengc, X., Kongd, Z., 2020. In situ major and trace element compositions of apatite from the Yangla skarn Cu deposit, Southwest China: implications for petrogenesis and mineralization. Ore Geol. Rev. 127, 103360.
Klaver, M., Carey, S., Nomikou, P., Smet, I., Godelitsas, A., Vroon, P., 2016. A distinct source and differentiation history for Kolumbo submarine volcano, Santorini volcanic field, Aegean arc: KOLUMBO SUBMARINE VOLCANO. Geochem. Geophys. Geosyst. 17, 3254–3273. https://doi.org/10.1002/2016GC006398.
Klaver, M., Matveev, S., Berndt, J., Lissenberg, C.J., Vroon, P.Z., 2017. A mineral and cumulate perspective to magma differentiation at Nisyros volcano, Aegean arc. Contrib. Mineral. Petrol. 172:95. https://doi.org/10.1007/s00410-017-1414-5.
Klaver, M., Blundy, J.D., Vroon, P.Z., 2018. Generation of arc rhyodacites through cumulate-melt reactions in a deep crustal hot zone: evidence from Nisyros volcano. Earth Planet. Sci. Lett. 497, 169–180. https://doi.org/10.1016/j.epsl.2018.06.019.
Limburg, E.M., Varekamp, J.C., 1991. Young pumice deposits on Nisyros, Greece. Bull. Volcanol. 54, 68–77. https://doi.org/10.1007/BF00278207.
Lodise, L., 1987. Petrology and Geochemistry of Nisyros Volcano (Dodecanese, Greece). M.A. Thesis. Wesleyan University, Middletown CT USA, p. 245.
Longchamp, C., Bonadonna, C., Bachmann, O., Skopelitis, A., 2011. Characterization of tephra deposits with limited exposure: the example of the two largest explosive eruptions at Nisyros volcano (Greece). Bull. Volcanol. 73, 1337–1352. https://doi.org/10.1007/s00445-011-0469-9.
Lucazeau, F., 2019. Analysis and Mapping of an Updated Terrestrial Heat Flow Data Set. Geochem. Geophys. Geosyst. 20, 4001–4024. https://doi.org/10.1029/2019GC008389.
Margari, V., Pyle, D.M., Bryant, C., Gibbard, P.L., 2007. Mediterranean tephra stratigraphy revisited: results from a long terrestrial sequence on Lesvos Island, Greece. J. Volcanol. Geotherm. Res. 163, 34–54.
Mastroianni, F., Braschi, E., Agostini, S., Di Salvo, S., Casalini, M., Vougioukalakis, G., Francalanci, L., 2021. Data on: Unveiling the Occurrence of Transient, Multi-Contaminated Mafic Magmas Refilling a Rhyolitic Reservoir in a Explosive Eruptions (Nisyros, Greece). Data in Brief, submitted.
Paola, Di, 1974. Volcanology and petrology of Nisyros Island (Dodecanese, Greece). Bull. Volcanol. 38, 944–987. https://doi.org/10.1007/BF02597100.
Papazachos, B.C., Panagiotopoulos, D.G., 1993. Normal faults associated with volcanic activity and deep rupture zones in the Southern Aegean volcanic arc. Bull. Geol. Greece 28, 243–252.
Peccerillo, A., Taylor, S.R., 1976. Geochemistry of eocene calc-alkaline volcanic rocks from the Kastamonu area, Northern Turkey. Contrib. Mineral. Petrol. 58, 63–81. https://doi.org/10.1007/BF00384745.
Plail, M., Barclay, J., Humphreys, M.C.S., Edmonds, M., Herd, R.A., Christopher, T.E., 2014. Chapter 18 Characterization of mafic enclaves in the erupted products of Soufrière Hills Volcano, Montserrat, 2009 to 2010. Geol. Soc. Lond. Mem. 39, 343–360. https://doi.org/10.1144/M39.18.
Plail, M., Edmonds, M., Woods, A.W., Barclay, J., Humphreys, M.C.S., Herd, R.A., Christopher, T.E., 2018. Mafic enclaves record syn-eruptive basalt intrusion and mixing. Earth Planet. Sci. Lett. 484, 30–40. https://doi.org/10.1016/j.epsl.2017.11.033.
Popa, R.G., Bachmann, O., Ellis, B.S., Degruyter, W., Tollan, P., Kyriakopoulos, K., 2019. A connection between magma chamber processes and eruptive styles revealed at Nisyros-Yali volcano (Greece). J. Volcanol. Geotherm. Res. 387, 106666 https://doi.org/10.1016/j.jvolgeores.2019.106666.
Popa, R.G., Guillong, M., Bachmann, O., Szymanowskia, D., Ellisa, B., 2020. U-Th zircon dating reveals a correlation between eruptive styles and repose periods at the Nisyros-Yali volcanic area, Greece. Chem. Geol. 555, 119830 https://doi.org/10.1016/j.chemgeo.2020.119830.
Ridolfi, F., 2021. Amp-TB2: an updated model for calcic amphibole thermobarometry. Minerals 11, 324. https://doi.org/10.3390/min11030324.
Sato, H., Holts, F., Botcharnikov, R.E., Nakada, S., 2017. Intermittent generation of mafic enclaves in the 1991–1995 dacite of Unzen Volcano recorded in mineral chemistry. Contrib. Mineral. Petrol. 172, 22. https://doi.org/10.1007/s00410-017-1335-3.
Seymour, K., Vlassopoulos, D., 1992. Magma mixing at Nisyros volcano, as inferred from incompatible trace-element systematics. J. Volcanol. Geotherm. Res. 50, 273–299. https://doi.org/10.1016/0377-0273(92)90097-W.
Shu, X., Liu, Y., 2019. Fluid inclusion constraints on the hydrothermal evolution of the Dalucao Carbonatite-related REE deposit, Sichuan Province, China. Ore Geol. Rev. 107, 41–57. https://doi.org/10.1016/j.oregeorev.2019.02.014.
Smith, P.E., York, D., Chen, Y., Evensen, N.M., 1996. Single crystal 40Ar-39Ar dating of a late Quaternary paroxysm on Kos, Greece: concordance of terrestrial and marine ages. Geophys. Res. Lett. 23, 3047–3050. https://doi.org/10.1029/96GL02759.
Spandler, C., Martin, L.H.J., Pettke, T., 2012. Carbonate assimilation during magma evolution at Nisyros (Greece), South Aegean Arc: evidence from clinopyroxenite xenoliths. Lithos 146–147, 18–33. https://doi.org/10.1016/j.lithos.2012.04.029.
Spera, F.J., Bohrson, W.A., 2001. Energy-Constrained Open-System Magmatic Processes III: Energy-Constrained Recharge, Assimilation and Fractional Crystallization (EC-RAFC) 41.
Tibaldi, A., Pasquarè, F.A., Papanikolaou, D., Nomikou, P., 2008. Tectonics of the Nisyros island, Greece, by field and offshore data, and analogue modelling. J. Struct. Geol. 30 (12), 1489–1506.
Tomlinson, E.L., Kinvig, H.S., Smith, V.C., Blundy, J.D., Gottsmann, J., Muller, W., Menzies, M.A., 2012. The upper and lower Nisyros Pumices: revisions to the mediterranean tephrostratigraphic record based on micron-beam glass geochemistry. J. Volcanol. Geotherm. Res. 243, 69–80.
Vanderkluysen, L., Volentik, A., Principe, C., Hunziker, J.C., Hernandez, J., 2005. 6. Nisyros' volcanic evolution: the growth of a strato-volcano. In book: the Geology, Geochemistry and Evolution of Nisyros Volcano (Greece). Implications for the Volcanic Hazards. Mém. Géol. (Lausanne) 44, 100–106.
Varekamp, J.C., 1993. Some remarks on volcanic vent evolution during plinian eruptions. J. Volcanol. Geotherm. Res. 54, 309–318. https://doi.org/10.1016/0377-0273(93)90069-4.

Volentik, A., Vanderkluisen, L., Prinicpe, C., 2002. Stratigraphy of the Caldera walls of Nisyros volcano, Greece. Eclo. Geol. Helv. 95 (2), 223–235. https://doi.org/10.5169/seals-168956.

Volentik, A.C.M., Vanderkluysen, L., Principe, C., Hunziker, J.C., 2005. 3. Stratigraphy of Nisyros Volcano (Greece) in book: the Geology, Geochemistry and Evolution of Nisyros Volcano (Greece). Implications for the Volcanic Hazards. Mém. Géol. (Lausanne) 44, 26–66.

Vougioukalakis, G., 1993. Volcanic stratigraphy and evolution of Nisyros island. Bull. Geol. Soc. Greece 28 (2), 239–258.

Wyers, G.P., Barton, M., 1989. Polybaric Evolution of Calc-alkaline Magmas from Nisyros, Southeastern Hellenic Arc, Greece. J. Petrol. 30 (1), 1–37.

Zellmer, G.F., Turner, S.P., 2007. Arc dacite genesis pathways: evidence from mafic enclaves and their hosts in Aegean lavas. Lithos 95, 346–362. https://doi.org/10.1016/j.lithos.2006.08.002.